Inorganic Chemistry

Article

pubs.acs.org/IC

# Stereochemical Consequences of Oxygen Atom Transfer and Electron Transfer in Imido/Oxido Molybdenum(IV, V, VI) Complexes with Two Unsymmetric Bidentate Ligands

Kristina Hüttinger,[†] Christoph Förster,[†] Timo Bund,[‡] Dariush Hinderberger,[‡] and Katja Heinze*[,†]

[†]Institute of Inorganic Chemistry and Analytical Chemistry, Johannes Gutenberg-University of Mainz, Duesbergweg 10-14, 55128 Mainz, Germany

[‡]Max Planck Institute for Polymer Research, Ackermannweg 10, 55128 Mainz, Germany

Supporting Information

**ABSTRACT:** Two equivalents of the unsymmetrical Schiff base ligand $(\mathbf{L}^{t\mathbf{Bu}})^-$ (4-*tert*-butyl phenyl(pyrrolato-2-ylmethylene)amine) and $MoCl_2(N\mathit{t}Bu)O(dme)$ (dme = 1,2-dimethoxyethane) gave a single stereoisomer of a mixed imido/oxido $Mo^{VI}$ complex $\mathbf{2}^{t\mathbf{Bu}}$. The stereochemistry of $\mathbf{2}^{t\mathbf{Bu}}$ was elucidated using X-ray diffraction, NMR spectroscopy, and DFT calculations. The complex is active in an oxygen atom transfer (OAT) reaction to trimethyl phosphane. The putative intermediate five-coordinate $Mo^{IV}$ imido complex coordinates a $PMe_3$ ligand, giving the six-coordinate imido phosphane $Mo^{IV}$ complex $\mathbf{5}^{t\mathbf{Bu}}$. The stereochemistry of $\mathbf{5}^{t\mathbf{Bu}}$ is different from that of $\mathbf{2}^{t\mathbf{Bu}}$ as shown by NMR spectroscopy, DFT calculations, and X-ray diffraction. Single-electron oxidation of $\mathbf{5}^{t\mathbf{Bu}}$ with ferrocenium hexafluorophosphate gave the stable cationic imido phosphane $Mo^V$ complex $[\mathbf{5}^{t\mathbf{Bu}}]^+$ as the $PF_6^-$ salt. EPR spectra of $[\mathbf{5}^{t\mathbf{Bu}}](\mathbf{PF_6})$ confirmed the presence of $PMe_3$ in the coordination sphere. Single-crystal X-ray diffraction analysis of $[\mathbf{5}^{t\mathbf{Bu}}](\mathbf{PF_6})$ revealed that electron transfer occurred under retention of the stereochemical configuration. The rate of OAT, the outcome of the electron transfer reaction, and the stabilities of the imido complexes presented here differ dramatically from those of analogous oxido complexes.

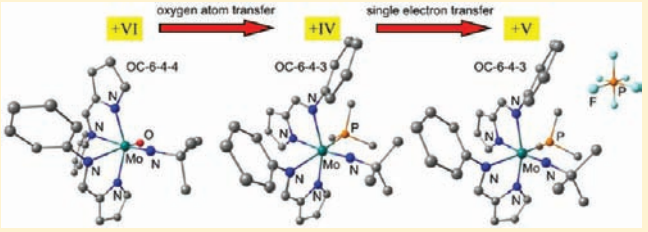


## INTRODUCTION

Oxygen atom transfer OAT[1] as seen, e.g., in molybdenum-containing oxotransferases[2,3] is very well studied using model chemistry.[4,5] The oxygen atom is transferred from a $[Mo^{VI}{=}O]$ species to the substrate giving a $[Mo^{IV}]$ species, and the oxygenated substrate, e.g., $SO_4^{2-}$, is formed from $SO_3^{2-}$.[6] We[7−9] and others[4,5] observed that in some reactions employing dioxido $Mo^{VI}O_2(X{\cap}Y)_2$ model complexes, e.g., of type **A** (Chart 1), as oxygen atom donor the resulting five-coordinate $Mo^{IV}O(X{\cap}Y)_2$ species form a $\mu$-oxido dimer $(X{\cap}Y)_2(O)Mo^V{-}O{-}Mo^V(O)(X{\cap}Y)_2$ as very stable intermediate by comproportionation with the starting material. This is a quite general phenomenon using uncharged and sterically less congested complexes.[4,5] With excess substrate, e.g., $PR'_3$, the vacant coordination site of the intermediate $Mo^{IV}O(X{\cap}Y)_2$ species can be filled by the phosphane substrate.[7−10] When two dissymmetric chelate ligands X∩Y are employed several stereoisomers $Mo(X{\cap}Y)_2(O)(PR'_3)$ are conceivable. We were able to deduce the stereochemistry of such molybdenum(IV) phosphane complexes by NMR spectroscopy and DFT calculations for complexes of dissymmetric imino pyrrolato chelate ligands $(L^R)^-$ (Chart 1; R = $OSiMe_3$).[7−9]

To close a catalytic cycle the two-electron-reduced molybdenum(IV) species has to be reoxidized to molybdenum(VI) via molybdenum(V) complexes in two single-electron transfer (SET) oxidation steps. One-electron oxidation of $Mo^{IV}(L^R)_2(O)(PR'_3)$ to the molybdenum(V) species $[Mo^V(L^R)_2(O)(PR'_3)]^+$ resulted in rapid loss of the coordinated phosphane $PR'_3$ (R′ = Me, Ph).[9] However, neither $Mo^{IV}$ species nor mononuclear $Mo^V$ species could be characterized in this system by X-ray diffraction methods so far due to solubility and stability reasons. We therefore decided (i) to improve the solubility of the complexes by introducing a *tert*-butyl group at the chelate ligand $HL^{t\mathrm{Bu}}$ and (ii) to modify solubility and electronics by replacing one oxido ligand by a *tert*-butyl imido ligand. In this report we describe our attempts to stabilize and characterize mononuclear $Mo^{IV}$ and $Mo^V$ complexes with imido ligands and two dissymmetric chelate ligands X∩Y. Parallel to our work on mixed imido/oxido complexes for oxygen atom transfer studies the group of Mösch-Zanetti recently reported the synthesis of $Mo^{VI}O(N\mathit{t}Bu)(X{\cap}Y)_2$ complexes with bidentate $\beta$-diketiminato supporting ligands (Chart 1, **B**).[11] Six-coordinate mixed imido/oxido complexes **C1** and **C2** with tetradentate salpen and salen ligands have also been reported by Sullivan (Chart 1).[12] Tetrahedral and pseudotetrahedral $Mo^{VI}$ complexes with a mixed imido/oxido donor set have also been reported.[18−21] As can be seen from Chart 1, the

**Received:** December 1, 2011
**Published:** March 20, 2012

ACS Publications © 2012 American Chemical Society



dx.doi.org/10.1021/ic202588u | *Inorg. Chem.* 2012, 51, 4180−4192

**Chart 1. Ligands $(L^R)^-$ and Dioxido Molybdenum(VI) Complexes A of Bidentate Imino Pyrrolato Chelate Ligands $(L^R)^-$,[7−9] Imido/Oxido Molybdenum(VI) Complexes B of Bidentate β-Diketiminato Ligands,[11] and Imido/Oxido Molybdenum(VI) Complexes C1/C2 of Tetradentate Schiff Base Ligands[12] [a]**

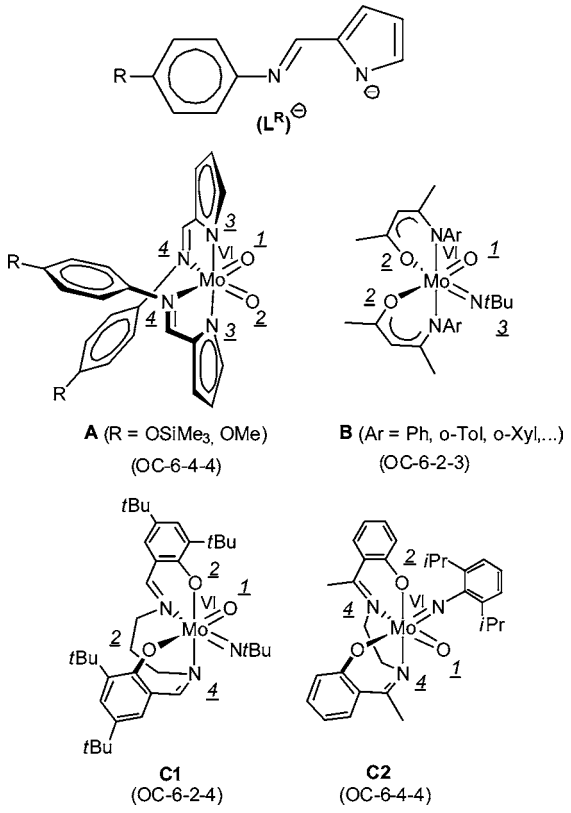


[a]The underlined numbers indicate the CIP priority for the stereodescriptor.[13−17]

stereochemistry (**C1**, **C2**)[13−17] is not easily predicted in six-coordinate imido/oxido $Mo^{VI}$ complexes. Even less is known about the stereochemistry of six-coordinate $Mo^{IV}$ and $Mo^{V}$ complexes with dissymmetric X∩Y chelate ligands. To the best of our knowledge, a detailed stereochemical and electronic analysis of $Mo^{IV}$ and $Mo^{V}$ complexes derived from $Mo^{VI}O(NtBu)(X∩Y)_2$ complexes by OAT and SET has not been reported yet.

## EXPERIMENTAL SECTION

**General Procedures.** All reactions were performed under an inert atmosphere (Schlenk techniques, glovebox). THF was distilled from potassium, diethyl ether, petroleum ether 40−60 °C, triethyl amine, and acetonitrile from calcium hydride. $MoCl_2O_2(dme)$[22] and $MoCl_2(NtBu)O(dme)$[20,23] were prepared according to literature procedures. All other reagents were used as received from commercial suppliers (Acros, Sigma-Aldrich). NMR spectra were recorded on a Bruker Avance DRX 400 spectrometer at 400.31 ($^1$H), 100.66 ($^{13}$C{$^1$H}), 162.05 ($^{31}$P{$^1$H}), and 40.56 MHz ($^{15}$N). All resonances are reported in ppm versus the solvent signal as internal standard [$d_8$-THF ($^1$H: δ = 1.24, 3.57; $^{13}$C: δ = 25.5, 67.7 ppm)], versus external $H_3PO_4$ (85%) ($^{31}$P: δ = 0 ppm) or versus external $CH_3NO_2$ (90% in $CDCl_3$) ($^{15}$N: δ = 380.23 ppm). $^{15}$N data are reported vs liquid $NH_3$ as reference (δ = 0 ppm). IR spectra were recorded with a BioRad Excalibur FTS 3100 spectrometer as KBr disks. Electrochemical experiments were carried out on a BioLogic SP-50 voltammetric analyzer using platinum wires as counter and working electrodes and a 0.01 *m* $Ag/AgNO_3$ electrode as reference electrode. Cyclic voltammetry measurements were carried out at a scan rate of 50−100 mV $s^{-1}$ using 0.1 *m* $(nBu_4N)(B(C_6F_5)_4)$ as supporting electrolyte in THF. Potentials are referenced to the ferrocene/ferrocenium couple ($E_{1/2}$ = 270 ± 5 mV under the experimental conditions). UV−vis−NIR spectra were recorded on a Varian Cary 5000 spectrometer using 1.0 cm cells (Hellma, suprasil). FD mass spectra were recorded on a FD Finnigan MAT90 spectrometer. ESI mass spectra were recorded on a Micromass Q-TOF-Ultima spectrometer. X-band CW EPR spectra were recorded on a Magnettech MS 300 spectrometer with a frequency counter Hewlett-Packard 5340A at a microwave frequency of 9.39 GHz in THF or frozen THF solution (77 K). $Mn^{2+}$ in ZnS was used as external standard. Simulations were performed with the program package EasySpin.[24] Details of the HYSCORE experiments can be found in the Supporting Information. Elemental analyses were performed by the microanalytical laboratory of the chemical institutes of the University of Mainz.

**Crystal Structure Determination.** Intensity data were collected with a Bruker AXS Smart1000 CCD diffractometer with an APEX II detector and an Oxford cooling system and corrected for absorption and other effects using Mo Kα radiation (λ = 0.71073 Å) at 173(2) K. Diffraction frames were integrated using the SAINT package, and most were corrected for absorption with MULABS.[25,26] Structures were solved by direct methods and refined by the full-matrix method based on $F^2$ using the SHELXTL software package.[27,28] All non-hydrogen atoms were refined anisotropically, while the positions of all hydrogen atoms were generated with appropriate geometric constraints and allowed to ride on their respective parent carbon atoms with fixed isotropic thermal parameters. Crystallographic data (excluding structure factors) for the structures reported in this paper have been deposited with the Cambridge Crystallographic Data Centre as supplementary publication nos. CCDC-831113 ($HL^{tBu}$), 831108 ($1^{tBu}$), 831109 ($2^{tBu}$), 831110 ($4^{tBu}$), 831112 ($5^{tBu}$), and 831111 ($[5^{tBu}](PF_6)$). Copies of the data can be obtained free of charge on application to CCDC, 12 Union Road, Cambridge CB2 1EZ, U.K. (fax (0.44) 1223-336-033; e-mail deposit@ccdc.cam.ac.uk).

Density functional calculations were carried out with the Gaussian03/DFT[29] series of programs. The B3LYP formulation of density functional theory was used employing the LANL2DZ basis set with d-type polarization functions on O (ζ = 1.154), N (ζ = 0.864), and P (ζ = 0.340) for geometry optimization.[30] No symmetry constraints were imposed on the molecules. For calculations of EPR parameters the EPR-II basis set[31] was used for C, H, and N, the WTBS basis set[32] for Mo, and 6-311++G(2d,2p) for P. For some calculations a solvent model was employed (integral equation formalism polarizable continuum model; IEFPCM; THF).

**Synthesis of $HL^{tBu}$.** 1*H*-Pyrrole-2-carbaldehyde (2 g, 21.03 mmol), 4-*tert*-butylaniline (3.35 mL, 21.03 mmol), $MgSO_4$ (2 g, 16.61 mmol), and ethyl acetate (100 mL) were heated under reflux for 4 h. The suspension was filtered while hot, and the solvent was removed under reduced pressure. The resulting orange-colored oil solidified upon cooling, and the solid was recrystallized from acetonitrile, giving pale yellow crystals in 75% yield (3.56 g, 15.72 mmol). Mp 116 °C. $^1$H NMR ($d_8$-THF): δ = 11.09 (br s, 1H, NH), 8.27 (s, 1H, $H^7$), 7.37 (d, 2H, $H^{3,5}$, $^3J_{HH}$ = 8.8 Hz), 7.10 (d, 2H, $H^{2,6}$, $^3J_{HH}$ = 8.8 Hz), 6.93 (s, 1H, $H^{11}$), 6.60 (dvd, 1H, $H^9$), 6.20 (dvd, 1H, $H^{10}$), 1.33 (s, 9H, $CH_3$). $^{13}$C{$^1$H} NMR ($d_8$-THF): δ = 151.2 (s, $C^1$), 150.1 (s, $C^7$), 148.6 (s, $C^4$), 132.5 (s, $C^8$), 126.7 (s, $C^{3,5}$), 123.8 (s, $C^{11}$), 121.3 (s, $C^{2,6}$), 116.8 (s, $C^9$), 110.5 (s, $C^{10}$), 35.2 (s, $C^q$), 32.1 (s, $CH_3$). $^{15}$N NMR ($d_8$-THF): δ = 285.6 ($N^p$), 199.8 ($N^i$). IR (KBr): ν = 3131 (w, NH), 2953 (m, $CH_3$), 1618 (m, C=N), 1587 (s), 1500 (m), 1418 (m), 1034 (m) $cm^{-1}$. UV−vis (THF): λ = 329 (22 560 $M^{-1}$ $cm^{-1}$) nm. MS (FD): *m*/*z* (%) = 226.2 (100, $M^+$). Anal. Calcd. for $C_{15}H_{18}N_2$ (226.31): C, 79.61; H, 8.02; N, 12.38. Found: C, 79.38; H, 8.16; N, 12.16.

**Synthesis of $1^{tBu}$.** The ligand $HL^{tBu}$ (346 mg, 1.19 mmol) was dissolved in THF (20 mL) and deprotonated with triethyl amine (1.0 mL, 7.14 mmol) for 30 min. In a separate flask $MoCl_2O_2(dme)$[22] (539 mg, 2.38 mmol) was dissolved in THF (50 mL), and the deprotonated ligand was added. After heating to reflux for 3 h the suspension was filtered, and the red filtrate was dried under reduced pressure. The


dx.doi.org/10.1021/ic202588u | Inorg. Chem. 2012, 51, 4180−4192

product was washed three times with methanol and dried under reduced pressure, giving a red crystalline solid in 81% yield (555 mg, 0.96 mmol). Mp 199 °C. $^1$H NMR ($d_8$-THF): $\delta$ = 7.95 (s, 1H, H$^7$), 7.25 (s, 1H, H$^{11}$), 7.16 (d, $^3J_{HH}$ = 8.43 Hz, 2H, H$^{3,5}$), 6.99 (d, $^3J_{HH}$ = 8.43 Hz, 2H, H$^{2,6}$), 6.35 (d, 1H, H$^9$), 6.08 (dd, 1H, H$^{10}$), 1.26 (s, 9H, CH$_3$). $^{13}$C{$^1$H} NMR ($d_8$-THF): $\delta$ = 158.6 (s, C$^7$), 149.4 (s, C$^4$), 147.2 (s, C$^1$), 144.0 (s, C$^{11}$), 140.1 (s, C$^8$), 126.0 (s, C$^{3,5}$), 122.4 (s, C$^{2,6}$), 120.0 (s, C$^9$), 115.2 (s, C$^{10}$), 35.2 (s, C$^q$), 31.8 (s, CH$_3$). $^{15}$N NMR ($d_8$-THF): $\delta$ = 248.3 (N$^i$), 215.1 (N$^p$). IR (KBr): $\nu$ = 2959 (m, CH$_3$), 1606 (m, C=N), 1581 (s), 1500 (m), 1431 (m), 1399 (s), 1296 (m), 1038 (m), 928 (m, Mo=O), 902 (m, Mo=O) cm$^{-1}$. UV–vis (THF): $\lambda$ = 235 (32 345), 303 (66 760), 436 (9440 M$^{-1}$ cm$^{-1}$) nm. MS (FD): $m/z$ (%) = 578.5 (76, M$^+$). CV (THF): $E_p$ = −0.86 V (irr). Anal. Calcd for $C_{30}H_{34}N_4O_2Mo$ (578.55): C, 62.28; H, 5.92; N, 9.68. Found: C, 60.93; H, 6.18; N, 9.50.

**Synthesis of 2$^{tBu}$.** The ligand **HL$^{tBu}$** (1.32 g, 5.8 mmol) was dissolved in THF (15 mL) and deprotonated with triethyl amine (2.4 mL, 17 mmol) for 30 min. In a separate flask $MoCl_2$(N*t*Bu)O-(dme)[20,23] (1.0 g, 2.9 mmol) was dissolved in THF (50 mL), and the deprotonated ligand was added. After heating to reflux for 7 h the suspension was filtered, and the red filtrate was dried under reduced pressure (95% raw yield). The product was washed with petroleum ether 40–60 °C (1:1), giving an orange-colored crystalline solid in 50% yield (950 mg, 1.5 mmol). Mp 174 °C. $^1$H NMR ($d_8$-THF): $\delta$ = 7.89 (s, 1H, H$^{7\prime}$), 7.76 (s, 1H, H$^7$), 7.28 (m, 1H, H$^{11\prime}$), 7.14 (m, 1H, H$^{11}$), 7.11 (d, $^3J_{HH}$ = 8.6 Hz, 2H, H$^{3\prime,5\prime}$), 7.08 (d, $^3J_{HH}$ = 8.5 Hz, 2H, H$^{3,5}$), 6.99 (d, $^3J_{HH}$ = 8.5 Hz, 2H, H$^{2\prime,6\prime}$), 6.78 (d, $^3J_{HH}$ = 8.5 Hz, 2H, H$^{2,6}$), 6.34 (dvd, 1H, H$^9$), 6.27 (dvd, 1H, H$^{9\prime}$), 6.11 (dvd, 1H, H$^{10}$), 6.06 (dvd, 1H, H$^{10\prime}$), 1.50 (s, 9H, NC(CH$_3$)), 1.25 (2 s, 18H, CH$_3$/CH$_3$′). $^{13}$C{$^1$H} NMR ($d_8$-THF): $\delta$ = 157.4 (s, C$^7$), 156.6 (s, C$^{7\prime}$), 148.8 (s, C$^{4\prime}$), 148.4 (s, C$^4$), 148.1 (s, C$^1$), 147.1 (s, C$^{1\prime}$), 143.2 (s, C$^{11\prime}$), 142.2 (s, C$^{11}$), 140.9 (s, C$^{8\prime}$), 139.1 (s, C$^8$), 125.8 (pd, C$^{3,5,3\prime,5\prime}$), 122.4 (s, C$^{2,6}$), 122.0 (s, C$^{2\prime,6\prime}$), 118.9 (s, C$^{9\prime}$), 118.2 (s, C$^9$), 114.3 (s, C$^{10\prime}$), 114.2 (s, C$^{10}$), 35.1 (s, C$^{q,q\prime}$), 31.9 (s, CH$_3$, CH$_3$′), 30.2 (s, NC–CH$_3$), 73.0 (s, NC–CH$_3$). $^{15}$N NMR ($d_8$-THF): $\delta$ = 477.4 (N$^{imido}$), 253.2 (N$^a$), 242.6 (N$^i$), 213.3 (N$^{tp}$), 205.1 (N$^p$). IR (KBr): $\nu$ = 2961 (m, CH$_3$), 1580 (s), 1518 (m), 1433 (w), 1395 (m), 1298 (m), 1039 (m), 897 (s, Mo=O) cm$^{-1}$. UV–vis (THF): $\lambda$ = 296 (16 780), 395 (8335 M$^{-1}$ cm$^{-1}$) nm. MS (FD): $m/z$ (%) = 633.4 (86, M$^+$). CV (THF): $E_p$ = −0.87 V (irr). Anal. Calcd for $C_{34}H_{43}N_5OMo$ (633.67): C, 64.44; H, 6.84; N, 11.05. Found: C, 63.34; H, 5.96; N, 11.04.

**Synthesis of 4$^{tBu}$.** Dioxido complex **1$^{tBu}$** (360 mg, 0.55 mmol) was dissolved in THF (20 mL), and trimethylphosphane (1 M in THF, 3.11 mL, 3.02 mmol) was added. After stirring for 7 days at room temperature volatiles were removed under reduced pressure to give a green powder in 91% yield (320 mg, 0.50 mmol). Attempts to completely remove the phosphane oxide by recrystallization from THF failed. Mp 203 °C (dec.). $^1$H NMR ($d_8$-THF): $\delta$ = 8.00 (d, $^4J_{PH}$ = 2.3 Hz, 1H, H$^7$), 7.63 (bs, 1H, H$^{11}$), 7.50 (bs, 1H, H$^{7\prime}$), 7.24 (d, $^3J_{HH}$ = 8.7 Hz, 2H, H$^{3\prime,5\prime}$), 7.11 (d, $^3J_{HH}$ = 8.7 Hz, 2H, H$^{2\prime,6\prime}$), 7.08 (d, $^3J_{HH}$ = 8.5 Hz, 2H, H$^{3,5}$), 7.01 (d, $^3J_{HH}$ = 2.7 Hz, 2H, H$^9$), 6.61 (d, $^3J_{HH}$ = 8.5 Hz, 2H, H$^{2,6}$), 6.5 (dd, 1H, H$^{10}$), 6.33 (dd, 1H, H$^{9\prime}$), 6.32 (pd, 1H, H$^{10\prime}$), 5.80 (bs, 1H, H$^{11\prime}$), 1.34 (s, 9H, CH$_3$′), 1.31 (s, 9H, CH$_3$), 1.31 (d, $^2J_{PH}$ = 8.5 Hz, 9H, P(CH$_3$)$_3$). $^{13}$C{$^1$H} NMR ($d_8$-THF): $\delta$ = 158.0 (s, C$^7$), 151.9 (s, C$^{1\prime}$), 151.2 (s, C$^{7\prime}$), 150.9 (s, C$^1$), 148.8 (s, C$^4$), 148.7 (s, C$^{4\prime}$), 147.9 (s, C$^{11}$), 144.9 (s, C$^8$), 141.3 (s, C$^{8\prime}$), 138.5 (s, C$^{11\prime}$), 126.2 (s, C$^{3,5}$), 125.8 (s, C$^{3\prime,5\prime}$), 124.0 (s, C$^{2\prime,6\prime}$), 123.0 (s, C$^{2,6}$), 119.3 (s. C$^9$), 115.8 (s. C$^{9\prime}$), 114.9 (s. C$^{10}$), 113.6 (s. C$^{10\prime}$), 35.2 (pd, C$^{q,q\prime}$), 32.0 (s, CH$_3$, CH$_3$′), 16.4 (d, $^1J_{PC}$ = 23.4 Hz, P(CH$_3$)$_3$). $^{31}$P{$^1$H} NMR ($d_8$-THF): $\delta$ = 1.3 (s, major), −5.3 (s, minor) ppm. $^{31}$P NMR ($d_8$-THF): $\delta$ = 1.3 (m, major, $^2J_{PH}$ = 8.5 Hz, $^4J_{PH}$ = 2.3 Hz). $^{15}$N NMR ($d_8$-THF): $\delta$ = 236.6 (N$^i$, N$^a$), 230.3 (N$^{tp}$), 219.0 (N$^p$). IR (KBr): $\nu$ = 2960 (w, CH$_3$), 1506 (w), 1390 (w), 935 (m, Mo=O) cm$^{-1}$. UV–vis (THF): $\lambda$ = 303 (8160), 345 (8180), 386 (sh), 479 (1420), 610 (250), 715 (200 M$^{-1}$ cm$^{-1}$) nm. MS (FD): $m/z$ (%) = 638.4 (100, M$^+$). CV (THF): $E_p$ = −0.29 V (irr).

**Synthesis of 5$^{tBu}$.** Imido/oxido complex **2$^{tBu}$** (400 mg, 0.63 mmol) was dissolved in THF (10 mL), and trimethylphosphane (1 M in THF, 5.00 mL, 5.0 mmol) was added. After stirring for 4 days at room temperature volatiles were removed under reduced pressure to give a black powder in 74% yield (325 mg, 0.47 mmol). Repeated recrystallization with a high loss of material was necessary to obtain a product almost free of OPMe$_3$. Mp 133 °C (dec.). $^1$H NMR ($d_8$-THF): $\delta$ = 7.85 (d, $^4J_{PH}$ = 2.8 Hz, 1H, H$^7$), 7.37 (bs, 1H, H$^{11}$), 7.28 (bs, 1H, H$^{7\prime}$), 7.17 (d, $^3J_{HH}$ = 8.3 Hz, 2H, H$^{3,5}$), 7.15 (d, $^3J_{HH}$ = 8.3 Hz, 2H, H$^{3\prime,5\prime}$), 6.85 (d, $^3J_{HH}$ = 2.8 Hz, 1H, H$^9$), 6.79 (d, $^3J_{HH}$ = 8.6 Hz, 2H, H$^{2\prime,6\prime}$), 6.64 (d, $^3J_{HH}$ = 8.5 Hz, 2H, H$^{2,6}$), 6.31 (dd, $^3J_{HH}$ = 1.9 Hz, 1H, H$^{10}$), 6.30 (d, $^3J_{HH}$ = 3.4 Hz, 1H, H$^{9\prime}$), 5.85 (dd, $^3J_{HH}$ = 1.7 Hz, 1H, H$^{10\prime}$), 5.73 (bs, 1H, H$^{11\prime}$), 1.30 (2 s, 18H, CH$_3$/CH$_3$′), 1.24 (d, $^2J_{PH}$ = 7.8 Hz, 9H, P(CH$_3$)$_3$), 1.01 (s, 9H, NC(CH$_3$)). $^{13}$C{$^1$H} NMR ($d_8$-THF): $\delta$ = 157.9 (s, C$^7$), 153.8 (s, C$^{1\prime}$), 152.0 (s, C$^1$), 148.4 (s, C$^{4\prime}$), 148.2 (2 s, C$^{4,7\prime}$), 145.4 (s, C$^{11}$), 144.8 (s, C$^{8\prime}$), 142.2 (s, C$^8$), 136.2 (s, C$^{11\prime}$), 125.8 (s, C$^{3,5}$), 125.2 (s, C$^{3\prime,5\prime}$), 123.8 (s, C$^{2\prime,6\prime}$), 123.2 (s, C$^{2,6}$), 117.3 (s, C$^9$), 113.7 (s, C$^{9\prime}$), 112.9 (s, C$^{10}$), 112.7 (s, C$^{10\prime}$), 35.0 (2 s, C$^{q,q\prime}$), 31.8 (2 s, CH$_3$, CH$_3$′), 30.7 (s, NC–CH$_3$), 69.1 (s, NC–CH$_3$), 18.7 (d, $^1J_{PC}$ = 22.3 Hz, P(CH$_3$)$_3$). $^{31}$P{$^1$H} NMR ($d_8$-THF): $\delta$ = 9.2 (s) ppm. $^{31}$P NMR ($d_8$-THF): $\delta$ = 9.2 (m, $^2J_{PH}$ = 7.8 Hz, $^4J_{PH}$ = 2.8 Hz). $^{15}$N NMR ($d_8$-THF): $\delta$ = 273.7 (N$^{imido}$), 252.2 (N$^a$), 234.2 (N$^i$), 231.1 (N$^{tp}$), 212.0 (N$^p$). IR (KBr): $\nu$ = 2963 (w, CH$_3$), 1573 (s), 1506 (m), 1433 (w), 1389 (m), 1296 (m), 1035 (m) cm$^{-1}$. UV–vis (THF): $\lambda$ = 299 (10 820), 340 (10 080), 377 (sh), 490 (1465), 594 (1000), 735 (265 M$^{-1}$ cm$^{-1}$) nm. MS (FD): $m/z$ (%) = 693.5 (82, M$^+$). CV (THF): $E_{1/2}$ = −0.71 V (rev oxidation). Anal. Calcd for $C_{37}H_{52}N_5MoP$ (693.77): C, 64.06; H, 7.55; N, 10.09. Found: C, 63.03; H, 7.67; N, 10.55.

*Oxidation of 4$^{tBu}$.* Oxido phosphane complex **4$^{tBu}$** (50 mg, 0.076 mmol) was dissolved in THF (5 mL), and a suspension of ferrocenium hexafluorophosphate (26 mg, 0.078 mmol) in THF (5 mL) was added. After stirring for 12 h at room temperature the solvent was removed under reduced pressure, giving a dark brown product (55 mg, possibly several paramagnetic species of unknown composition, see text). EPR (THF, 298 K): $g_{iso}$ = 1.9459, $A_{iso}$($^{95/97}$ Mo) = 49.8 G. EPR (THF, 77 K): $g_{1,2,3}$ = 1.9618, 1.9555, 1.9362.

**Synthesis of [5$^{tBu}$](PF$_6$).** Imido phosphane complex **5$^{tBu}$** (100 mg, 0.144 mmol) was dissolved in THF (5 mL), and a suspension of ferrocenium hexafluorophosphate (47.7 mg, 0.144 mmol) in THF (5 mL) was added. After stirring for 12 h at room temperature the solvent was removed under reduced pressure, giving a black product, which was washed with petroleum ether 40–60 °C and repeatedly recrystallized from THF/petroleum ether 40–60 °C. The yield after the first recrystallization was 75 mg (0.09 mmol, 62%). Mp 151 °C (dec.). EPR (THF, 298 K): $g_{iso}$ = 1.9810, $A_{iso}$($^{95/97}$ Mo) = 40.3 G, $A_{iso}$($^{31}$P) = 28.7 G. EPR (THF, 77 K): $g_{1,2,3}$ = 1.9825, 1.9785, 1.9615, $A_{1,2,3}$($^{31}$P) = 23, 33, 29 G. HYSCORE (THF, 20 K): $A_{1,2,3}$($^{14}N_{large}$) = 1.5, 2.0, 3.8 G, $A_{1,2,3}$($^{14}N_{small,A}$) = 1.3, 1.4, 1.7 G, $A_{1,2,3}$($^{14}N_{small,B}$) = 0.8, 0.8, 0.9 G, $A_{1,2,3}$($^1$H) = 3.4, 4.1, 5.0 G, $A_{iso}$($^{14}N_{large}$) = 2.4 G, $A_{iso}$($^{14}N_{small,A}$) = 1.5 G, $A_{iso}$($^{14}N_{small,B}$) = 0.8 G, $A_{iso}$($^1$H) = 4.2 G. IR (KBr): $\nu$ = 2962 (w, CH$_3$), 1572 (m), 1506 (w), 1433 (w), 1390 (m), 1269 (m), 840 (s, PF) cm$^{-1}$. UV–vis (THF): $\lambda$ = 298 (29 865), 405 (12 815, sh), 532 (1165, sh), 787 (905 M$^{-1}$ cm$^{-1}$) nm. MS (ESI+): $m/z$ (%) = 693.3 (81, M$^+$). CV (THF): $E_{1/2}$ = −0.73 V (rev reduction). $\mu_{eff}$ (THF, 298 K) = 1.71 ± 0.05 $\mu_B$. Anal. Calcd for $C_{37}H_{52}N_5MoP_2F_6$ (838.73): C, 52.99; H, 6.25; N, 8.35. Found: C, 51.98; H, 7.34; N, 7.97.

## RESULTS AND DISCUSSION

All complex syntheses performed as well as compound abbreviations are summarized in Scheme 1.

**Synthesis and Properties of the Chelate Ligand and Its Mo(VI) Complexes.** The highly soluble chelate ligand **HL$^{tBu}$** is easily obtained by Schiff base condensation of pyrrole-2-carbaldehyde and 4-(*tert*-butyl)aniline in the presence of magnesium sulfate in high yield similar to comparable syntheses.[7,8] It crystallizes from CH$_3$CN in the space group *Cc* as colorless long bricks with two independent molecules in the unit cell (Figure 1). The two molecules differ only in the aryl torsion angles C7–C8–N1–C11 = −20.8(2)°/C24–C23–N3–C26 = −31.6(2)°, and they are linked by N–H···N


dx.doi.org/10.1021/ic202588u | *Inorg. Chem.* 2012, 51, 4180–4192

**Scheme 1. Synthesis of Molybdenum Complexes of Ligand $HL^{tBu}$ (R = *t*Bu) and Atom Numbering for NMR Assignments**

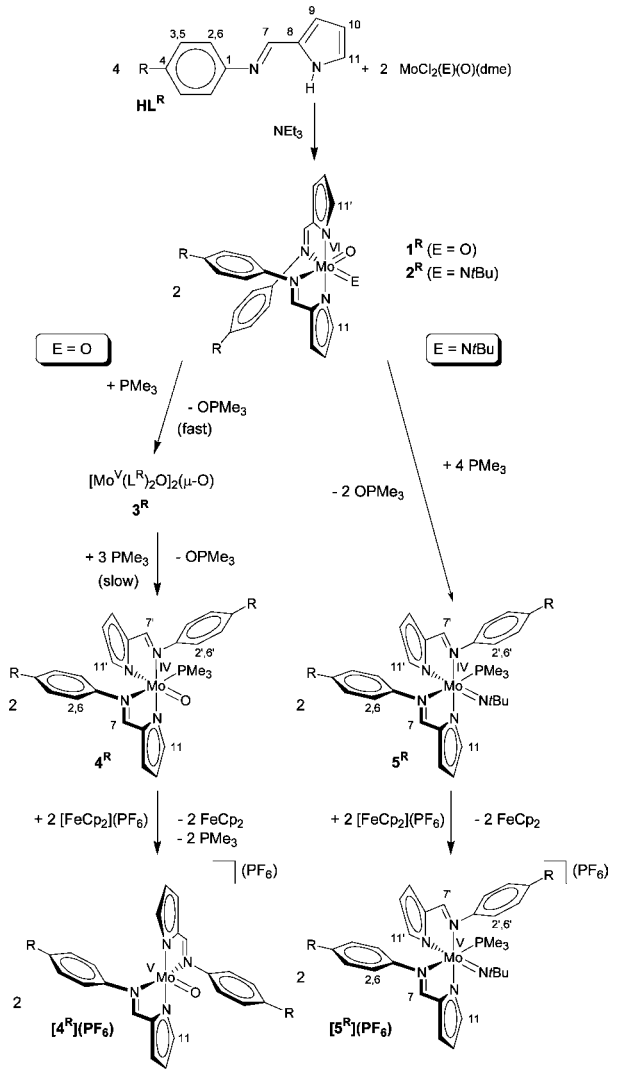


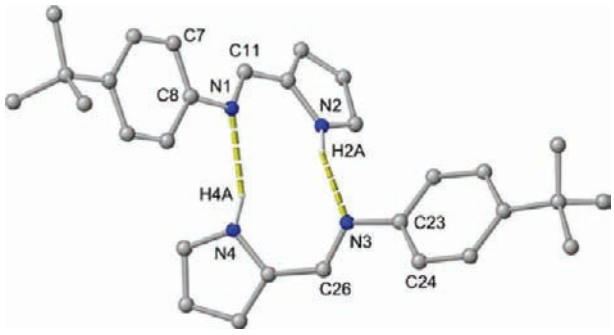


**Figure 1.** Molecular structure and intermolecular hydrogen bonding of $HL^{tBu}$ in the crystal (CH hydrogen atoms omitted for clarity).

hydrogen bonds to give a dimer with an $R^2_2(10)$ motif[33,34] (N2···N3 = 2.987(2) Å; N4···N1 = 3.008(2) Å).

The bis(chelate) dioxido complex $\mathbf{1}^{tBu}$ was prepared similar to literature procedures[7,8] for $\mathbf{1}^{R}$ (R = OMe, $OSiMe_3$) from $MoCl_2O_2(dme)$[12] and the chelate ligand $HL^{tBu}$ in the presence of triethyl amine as red crystalline solid. The mixed imido/oxido complex $\mathbf{2}^{tBu}$ was prepared from the convenient precursor complex $MoCl_2(NtBu)(O)(dme)$[20,23] and $HL^{tBu}$ in the presence of triethyl amine as yellow solid. Both *tert*-butyl-substituted complexes $\mathbf{1}^{tBu}$ and $\mathbf{2}^{tBu}$ are excellently soluble in typical organic solvents like THF or diethyl ether, which greatly facilitates purification, spectroscopic characterization, and crystallization.

The most stable stereoisomer of $\mathbf{1}^{R}$ is the OC-6-4-4 isomer[13−17] with the two oxido ligands in cis positions as expected for $d^0$ complexes and each oxido ligand trans to the imine nitrogen atoms of the chelate ligands.[8] In the infrared spectrum of the *tert*-butyl derivative $\mathbf{1}^{tBu}$ the absorptions of the two Mo═O vibrations are found at 928 and 902 $cm^{-1}$, consistent with the expected cis dioxido moiety.[7,8] The proton NMR spectrum of $\mathbf{1}^{tBu}$ displays a single signal set for two chelate ligands, suggesting the presence of one diastereomer with $C_2$ symmetry. Upon coordination of the chelate to molybdenum the resonance of proton $H^{11}$ experiences a large coordination shift to lower field from $\delta$ = 6.93 ppm to $\delta$ = 7.25 ppm, while the resonance of imine proton $H^7$ shifts from $\delta$ = 8.27 ppm to $\delta$ = 7.95 ppm. The nitrogen nuclei of ligand $HL^{tBu}$ resonate at $\delta$ = 199.8 ($N^i$ = $N^{imine}$) and 285.6 ppm ($N^p$ = $N^{pyrrolato}$). These resonances are considerably shifted to $\delta$ = 248.3 ($N^i$) and 215.1 ppm ($N^p$) in the $Mo^{VI}$ complex $\mathbf{1}^{tBu}$ (cf. $\mathbf{1}^{OSiMe3}$ [9]). Single-crystal X-ray structure analysis of $\mathbf{1}^{tBu}$ corroborates the proposed OC-6-4-4 stereochemistry (Figure 2). $\mathbf{1}^{tBu}$ crystallized from diethyl ether in the monoclinic space

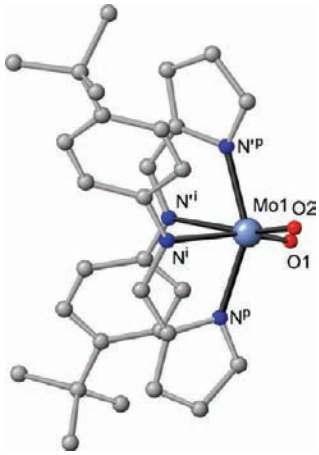


**Figure 2.** Molecular structure of $\mathbf{1}^{tBu}$ in the crystal (CH hydrogen atoms omitted for clarity).

group $P2_1/c$ with two independent molecules in the asymmetric unit (Table 1). DFT calculations (B3LYP, LANL2DZ with d-type polarization functions on O[30]) for the model system $\mathbf{1}^{H}$ are also in good agreement with the experimental metrical data (Table 2).[8]

In a previously reported mixed imido/oxido $Mo^{VI}(O)(NtBu)$(salpen) complex **C1** (Chart 1) the tetradentate salpen ligand with a $(CH_2)_3$ linker between the imino donor atoms induces an OC-6-2-4 configuration (imido/oxido cis to each other, oxido trans to phenolato, and imido trans to imine), while a salen ligand with a $(CH_2)_2$ linker between the imino donor atoms and a bulky aryl−imido ligand N(2,6-*i*Pr-$C_6H_3$) favors the OC-6-4-4 isomer **C2** (imido/oxido cis to each other, oxido trans to imine, and imido trans to phenolato).[12] Two bidentate $\beta$-diketiminato ligands induce OC-6-2-3 stereochemistry (complexes of type **B**, Chart 1).[11]


dx.doi.org/10.1021/ic202588u | *Inorg. Chem.* 2012, 51, 4180−4192

**Table 1. Crystallographic Data and Structure Refinement of $HL^{tBu}$, $1^{tBu}$, $2^{tBu}$, $4^{tBu}$, $5^{tBu}$, and $[5^{tBu}](PF_6)$**

| | $HL^{tBu}$ | $1^{tBu}$ | $2^{tBu}$ | $4^{tBu}$ | $5^{tBu}$ | $[5^{tBu}](PF_6)$ |
|---|---|---|---|---|---|---|
| empirical formula | $C_{15}H_{18}N_2$ | $C_{30}H_{34}MoN_4O_2$ | $C_{34}H_{43}MoN_5O$ | $C_{33}H_{43}MoN_4OP$ | $C_{37}H_{52}MoN_5P$ | $C_{45}H_{68}MoN_5O_2P_2F_6$ |
| fw | 226.31 | 578.55 | 633.67 | 638.62 | 693.75 | 982.92 |
| cryst syst | monoclinic | monoclinic | tetragonal | monoclinic | monoclinic | orthorhombic |
| space group | *Cc* | $P2_1/c$ | $I4_1/a$ | *C*2/*c* | $P2_1/n$ | *Pbca* |
| *a*/Å | 11.3992(5) | 16.2627(5) | 25.2905(8) | 35.703(7) | 11.8934(6) | 18.8771(9) |
| *b*/Å | 16.8185(7) | 25.0561(7) | 25.2905(8) | 7.4514(14) | 24.7875(12) | 19.6195(10) |
| *c*/Å | 13.8657(6) | 14.8107(5) | 21.4037(14) | 28.794(5) | 12.7566(7) | 26.9700(14) |
| *β*/deg | 97.3820(10) | 110.3530(10) | 90 | 122.153(5) | 94.515(2) | 90 |
| volume/Å$^3$ | 2636.3(2) | 5658.3(3) | 13690.0(11) | 6485(2) | 3749.1(3) | 9988.6(9) |
| *Z* | 8 | 8 | 16 | 8 | 4 | 8 |
| density (calcd), Mg m$^3$ | 1.140 | 1.358 | 1.230 | 1.308 | 1.229 | 1.307 |
| abs coeff, mm$^{-1}$ | 0.068 | 0.496 | 0.415 | 0.484 | 0.423 | 0.389 |
| *F*(000) | 976 | 2400 | 5312 | 2672 | 1464 | 4120 |
| cryst size, mm$^3$ | 0.65 × 0.44 × 040 | 0.26 × 0.22 × 0.08 | 0.06 × 0.02 × 0.02 | 0.15 × 0.03 × 0.02 | 0.33 × 0.30 × 0.12 | 0.15 × 0.05 × 0.02 |
| *θ* range for data collection | 2.42−25.23 | 2.28−27.96 | 2.22−27.89 | 2.29−28.07 | 2.29−28.07 | 2.39−27.92 |
| index ranges | $-13 \le h \le 13$ | $-21 \le h \le 21$ | $-33 \le h \le 33$ | $-46 \le h \le 46$ | $-15 \le h \le 15$ | $-24 \le h \le 24$ |
| | $-20 \le k \le 20$ | $-32 \le k \le 32$ | $-33 \le k \le 33$ | $-9 \le k \le 9$ | $-32 \le k \le 32$ | $-25 \le k \le 25$ |
| | $-16 \le h \le 16$ | $-19 \le h \le 19$ | $-28 \le h \le 28$ | $-36 \le h \le 37$ | $-16 \le h \le 16$ | $-35 \le h \le 35$ |
| no. of reflns collected | 12 407 | 65 502 | 110 537 | 37 366 | 43 312 | 215 807 |
| no. of indep reflns | 4555 | 13 533 | 8179 | 7840 | 9016 | 11 896 |
| $R_{int}$ | 0.0617 | 0.0932 | 0.2109 | 0.1764 | 0.0712 | 0.1033 |
| completeness to $\theta_{max}$ | 100.0 | 99.4 | 99.8 | 99.5 | 98.9 | 99.4 |
| max/min transmn | | 0.9614/0.8818 | 0.990/0.992 | 0.9904/0.9309 | 0.9510/0.8730 | 0.9923/0.9440 |
| goodness-of-fit on $F^2$ | 1.050 | 0.908 | 0.761 | 0.886 | 0.900 | 1.117 |
| final *R* indices [$I > 2\sigma(I)$]] | $R_1$ = 0.0323 | $R_1$ = 0.0412 | $R_1$ = 0.0381 | $R_1$ = 0.0622 | $R_1$ = 0.0334 | $R_1$ = 0.0562 |
| | $wR_2$ = 0.0817 | $wR_2$ = 0.0721 | $wR_2$ = 0.0567 | $wR_2$ = 0.1029 | $wR_2$ = 0.0666 | $wR_2$ = 0.1474 |
| *R* indices (all data) | $R_1$ = 0.0347 | $R_1$ = 0.0752 | $R_1$ = 0.1054 | $R_1$ = 0.1640 | $R_1$ = 0.0638 | $R_1$ = 0.0916 |
| | $wR_2$ = 0.0830 | $wR_2$ = 0.0824 | $wR_2$ = 0.0673 | $wR_2$ = 0.1185 | $wR_2$ = 0.0747 | $wR_2$ = 0.1602 |
| largest diff peak and hole, e/Å$^3$ | 0.137/−0.135 | 0.547/−0.805 | 0.347/−0.332 | 1.011/−0.613 | 0.425/−0.720 | 0.536/−0.562 |

**Table 2. Selected Bond Lengths (Angstroms) and Angles (degrees) of $1^{tBu}$, $2^{tBu}$, $4^{tBu}$, $5^{tBu}$, and $[5^{tBu}](PF_6)$**

| | $1^{tBu}$ (2 molecules) | $2^{tBu}$ | $4^{tBu}$ | $5^{tBu}$ | $[5^{tBu}](PF_6)$ |
|---|---|---|---|---|---|
| Mo1−O1 | 1.698(2)/1.702(2) | 1.705(2) | 1.686(4) | | |
| Mo1−O2 | 1.702(2)/1.704(2) | | | | |
| Mo1−$N^{imido}$ | | 1.731(2) | | 1.743(2) | 1.739(3) |
| Mo1−$N^{i}$ | 2.320(2)/2.349(2) | 2.375(2) | 2.182(4) | 2.220(2) | 2.198(3) |
| Mo1−$N^{p}$ | 2.081(2)/2.073(2) | 2.129(2) | 2.126(4) | 2.155(2) | 2.110(3) |
| Mo1−$N^{i}$ | 2.351(2)/2.353(2) | 2.401(2) | 2.213(4) | 2.201(2) | 2.143(3) |
| Mo1−$N^{p}$ | 2.066(2)/2.079(2) | 2.087(2) | 2.272(5) | 2.218(2) | 2.212(3) |
| Mo1−P1 | | | 2.482(2) | 2.4532(6) | 2.549(1) |
| Mo1−$N^{imido}$-$C^{imido}$ | | 159.1(2) | | 178.7(2) | 172.8(3) |
| O1−Mo1−O2 | 105.54(9)/106.0(1) | | | | |
| O1−Mo1−$N^{imido}$ | | 103.5(1) | | | |
| P1−Mo1−O1 | | | 92.3(1) | | |
| P1−Mo1−$N^{imido}$ | | | | 92.53(6) | 99.2(1) |

For our mixed imido/oxido complex $2^{tBu}$ DFT calculations on $2^{H}$ (B3LYP, LANL2DZ with d-type polarization functions on O and N[30]) suggest the OC-6-4-4 stereoisomer as the most stable one similar to the dioxido complex $1^{tBu}$ (Figure 3). The other plausible stereoisomers OC-6-3-4, OC-6-4-3, and OC-6-3-3 are calculated higher in energy by 6.7, 22.4, and 36.1 kJ mol$^{-1}$, respectively (Figure 3).

In any case, introduction of the imido ligand reduces the complex symmetry from $C_2$ ($1^{tBu}$) to $C_1$ ($2^{tBu}$). Thus, in the NMR spectra of $2^{tBu}$ two signal sets are expected for the two chelate ligands L and L′. For example, the resonances of $H^{11}$/$H^{11\prime}$ are found at $\delta$ = 7.14/7.28 ppm, and the resonances of $H^{7}$/$H^{7\prime}$ are observed at $\delta$ = 7.76/7.89 ppm. The $^{15}$N resonances of $2^{tBu}$ are recorded at $\delta$ = 242.6/253.2 ($N^{i}$/$N^{i}$), 205.1/213.3 ($N^{p}$/$N^{p}$), and 477.4 ppm ($N^{imido}$). Proton−proton, nitrogen−proton, and carbon−proton correlation spectroscopy allowed us to unambiguously assign all proton signals to the two different coordinated chelate ligands ($L^{tBu}$: $H^{2,6}$/$H^{3,5}$/$H^{7}$/$H^{9}$/$H^{10}$/$H^{11}$; $L'^{tBu}$: $H^{2',6'}$/$H^{3',5'}$/$H^{7'}$/$H^{9'}$/$H^{10'}$/$H^{11'}$). Several *inter-ligand* nuclear Overhauser contacts which are relevant for the relative ligand orientations are observed for $2^{tBu}$, namely, $H^{11'} \leftrightarrow H^{2,6}$, $H^{11'} \leftrightarrow H^{tBu,imido}$, $H^{7'} \leftrightarrow H^{2,6}$, and $H^{7} \leftrightarrow H^{2',6'}$. Some of these NOE contacts are indicated in Figure 3 for the calculated stereoisomers. The $H^{11'} \leftrightarrow H^{tBu,imido}$ correlation places the pyrrolato ring of $L'^{tBu}$ ($N^{p}$) in the cis position to the *tert*-butyl imido ligand with the $C^{11'}$−$H^{11'}$ vector oriented in the Mo=N-*t*Bu direction, i.e., the $N^{i}$ atom is located trans to N*t*Bu. This is fulfilled for the OC-6-4-4 and OC-6-3-4 isomers. A short $H^{11'}$


dx.doi.org/10.1021/ic202588u | *Inorg. Chem.* 2012, 51, 4180−4192

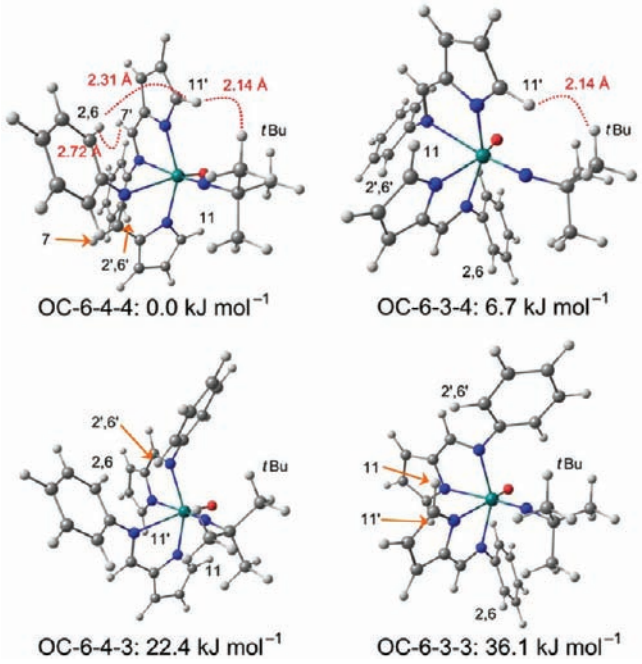


**Figure 3.** DFT-calculated stereoisomers of $\mathbf{2}^{H}$ together with relevant interligand H···H distances (shortest distance obtained by phenyl and *tert*-butyl rotations) and relative energies in kJ mol$^{-1}$.

↔ $H^{2,6}$ distance is found in the OC-6-4-4 isomer but not in the OC-6-3-4 isomer. The $H^{7'}$ ↔ $H^{2,6}$ and $H^{7}$ ↔ $H^{2',6'}$ NOEs place $N^{i}$ and $N^{ri}$ in close proximity, which is fulfilled in the OC-6-4-4 isomer (Figure 3). Thus, from the DFT-calculated H···H distances only the expected OC-6-4-4 isomer fits to the experimental data as all other isomers violate some of the NOE distance constraints.

Single crystals of $\mathbf{2}^{tBu}$ were grown from diethyl ether/petroleum ether 40−60° (1:1) at room temperature. $\mathbf{2}^{tBu}$ crystallized in the tetragonal space group $I4_1/a$ (Figure 4, Tables 1 and 2). Six-coordinate heteroleptic imido/oxido complexes are relatively unexplored with respect to structural data.[11,12] Recently, Mösch-Zanetti et al. reported the synthesis and structures of well-defined mixed imido/oxido complexes with $\beta$-ketiminato N, O chelate ligands.[11] They reported a slight elongation of the Mo═O bond length by replacing one oxido by an imido ligand for these complexes.[11] An analogous slight elongation is within experimental error when comparing the Mo═O bond lengths of $\mathbf{1}^{tBu}$ (1.698−1.704(2) Å) with that of $\mathbf{2}^{tBu}$ (1.705(2) Å) (Table 2). However, this slight elongation of the Mo═O bond is also reproduced by DFT calculations on $\mathbf{1}^{H}$ and $\mathbf{2}^{H}$ ($\mathbf{1}^{H}$, 1.713/1.715 Å; $\mathbf{2}^{H}$, 1.719 Å).

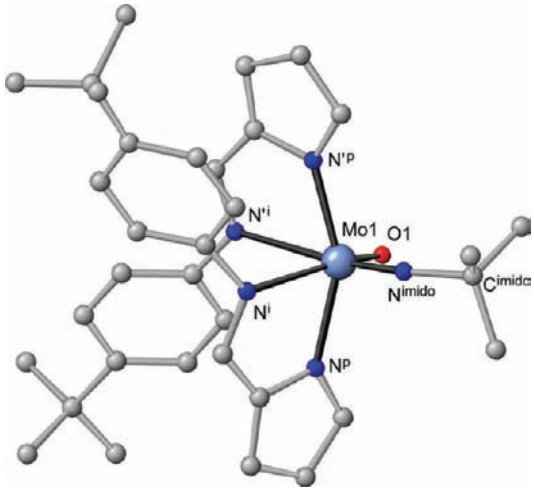


**Figure 4.** Molecular structure of $\mathbf{2}^{tBu}$ in the crystal (CH hydrogen atoms omitted for clarity).

The quite short Mo1═$N^{imido}$ bond length of 1.731(2) Å points to a significant triple-bond character (DFT $\mathbf{2}^{H}$, 1.746 Å). Mo═N distances in a similar range have been reported for six-coordinate imido/oxido complexes (type **B** complexes 1.742(2) and 1.734(6) Å[11] and complex **C1** 1.740(4) and 1.731(4) Å[12]). Almost linear imido ligands have been found for **B**-type complexes (175.6(2)°, 172.5(5)°)[11] and **C1** (174.2(4)°, 167.6(4)°)[12]. The Mo1═$N^{imido}$−$C^{imido}$ angle of the imido ligand of $\mathbf{2}^{tBu}$ amounts to 159° in the X-ray structure analysis of $\mathbf{2}^{tBu}$. DFT calculations on $\mathbf{2}^{H}$ suggest a very shallow potential for the Mo═N−C deformation.[35] A 140−180° bending deformation lies within 11 kJ mol$^{-1}$ (see Supporting Information, Figure S1). A minimum is calculated at 160°, in good agreement with the experimental value. This facile bending of the Mo═N−C angle should allow a nucleophilic associative attack at the oxido ligand in spite of the presence of the sterically demanding *tert*-butyl group at the imido nitrogen (vide infra). Additionally, the Mo1−$N^{ri}$ bond length trans to the imido ligand is significantly larger (2.394(3) Å) than the corresponding Mo1−$N^{i}$ bond lengths trans to oxido ligands (2.32−2.37 Å), which reflects the stronger trans influence of the N*t*Bu ligand as compared to the oxido ligand.[36] This trend is also observed in the DFT-calculated structures (2.493 Å trans to imido; 2.413−2.481 Å trans to oxido).

The energies of the Mo═O stretching vibrations have been calculated for $\mathbf{1}^{H}$ and for $\mathbf{2}^{H}$ by DFT methods (and scaled by 0.9614[37]) as 940/914 ($\mathbf{1}^{H\,8}$) and 910 cm$^{-1}$ ($\mathbf{2}^{H}$), in good agreement with the experimental data 928/902 ($\mathbf{1}^{tBu}$) and 897 cm$^{-1}$ ($\mathbf{2}^{tBu}$), Figure 5. From a structural and vibrational point of view the calculations reproduce and confirm the experimental data sufficiently well. Then, the electronic structures of the $d^0$ complexes $\mathbf{1}^{tBu}$ and $\mathbf{2}^{tBu}$ have been probed by UV−vis absorption spectroscopy and TD-DFT calculations. TD-DFT

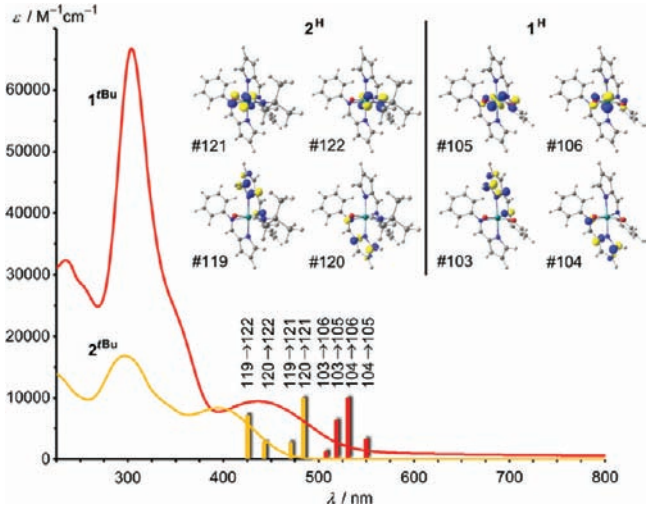


**Figure 5.** UV−vis spectra of $\mathbf{1}^{tBu}$ and $\mathbf{2}^{tBu}$ in THF; calculated low-energy transitions of $\mathbf{1}^{H}$ and $\mathbf{2}^{H}$ as stick representation; frontier Kohn−Sham molecular orbitals of $\mathbf{1}^{H}$ and $\mathbf{2}^{H}$ (contour value 0.1 au).


dx.doi.org/10.1021/ic202588u | *Inorg. Chem.* 2012, 51, 4180−4192

calculations have also been performed with inclusion of a solvent model (integral equation formalism polarizable continuum model; IEFPCM; THF). However, no significant improvement was noticed in the calculated spectra.

The red color of the dioxido complex $\mathbf{1}^{t\mathbf{Bu}}$ arises from an absorption band at $\lambda$ = 436 nm ($\varepsilon$ = 9440 $M^{-1}$ $cm^{-1}$), which is absent in the ligand $\mathbf{HL}^{t\mathbf{Bu}}$. It is assigned LMCT/LLCT in character. TD-DFT calculations on $\mathbf{1}^{\mathbf{H}}$ find an absorption band at 528 nm, which is composed of four transitions with similar energy ($\lambda$ = 508, 518, 531, 550 nm). All transitions involve the four frontier orbitals of the complex, namely, two occupied orbitals of the pyrrolato ligands (MO nos. 103, 104) and two $\pi^*$ orbitals of the $MoO_2$ unit (MO nos. 105, 106). The yellow imido/oxido complex $\mathbf{2}^{t\mathbf{Bu}}$ lacks characteristic absorption maxima in the visible region ($\lambda$ = 395 nm, $\varepsilon$ = 8335 $M^{-1}$ $cm^{-1}$; only tailing into the visible region). TD-DFT calculations on $\mathbf{2}^{\mathbf{H}}$ predict analogous transitions to $\mathbf{1}^{\mathbf{H}}$ involving the pyrrolato ligands (MO nos. 119, 120) and the Mo═O (MO no. 121) and Mo═N*t*Bu units (MO no. 122). However, these excitations occur at higher energy and with much more spread ($\lambda$ = 426, 443, 470, 483 nm) due to the larger energy difference $\Delta E$ of the acceptor orbital energies ($\mathbf{1}^{\mathbf{H}}$, $\Delta E$(105,106) = 0.10 eV; $\mathbf{2}^{\mathbf{H}}$, $\Delta E$(121,122) = 0.24 eV). These effects explain the less intense color of the imido/oxido complex.

**Oxygen Atom Transfer and Stereochemistry of Mo(IV) Products.** The OAT from dioxido complexes $\mathbf{1}^{\mathbf{R}}$ (R = $OSiMe_3$, O−Si(*i*Pr)$_2$−polymer) to phosphanes $PMe_nPh_{3-n}$ has been recently investigated experimentally[7,9] and on a theoretical basis (R = H).[8] After associative attack of the phosphane at a molybdenum-bound oxido ligand, formation, and dissociation of the phosphane oxide a five-coordinate molybdenum(IV) intermediate is formed. Its vacant coordination site is either filled with a remaining starting $Mo^{VI}$ dioxido complex forming a binuclear oxido bridged complex $L^R_2(O)Mo^V{-}O{-}Mo^V(O)L^R_2$ ($\mathbf{3}^{\mathbf{R}}$) or by excess substrate $PMe_nPh_{3-n}$ ($n$ = 1 − 3) after longer reaction times.[10] For the resulting phosphane complexes $\mathbf{4}^{\mathbf{H}}$ (with R = H and $n$ = 3; $PMe_3$) several stereoisomers have been considered by DFT calculations. The OC-6-3-3 and OC-6-4-3 isomers of $\mathbf{4}^{\mathbf{H}}$ are the lowest energy isomers with very similar energy, while the OC-6-4-4 isomer is calculated significantly higher in energy.[8] On the basis of NOE contacts and DFT calculations the OC-6-4-3 isomer of $\mathbf{4}^{\mathbf{OSiMe3}}$ is preferred in THF solution.[7−9]

For the reaction of $\mathbf{1}^{t\mathbf{Bu}}$ with $PMe_3$ similar results were obtained (Scheme 1). Due to the excellent solubility of the complexes two resonances for two stereoisomers $\mathbf{4}^{t\mathbf{Bu}}$ were discernible in the $^{31}P\{^1H\}$ NMR spectrum ($\delta$ = 1.3 and −5.3 ppm in a ratio ≈ 5 : 2). These two isomers can be distinguished in the $^1H$ NMR spectrum as well (four different signal sets for the chelate ligands are observed). All resonances of the major isomer could be assigned by correlation spectroscopy. The resonance of proton $H^7$ is split to a doublet with $^4J_{PH}$ = 2.3 Hz. The P−H correlation spectrum confirms that this doublet arises from coupling to phosphorus ($\delta$ = 1.3 ppm; see Supporting Information, Figure S8). Weaker cross peaks of the phosphorus nucleus are found to $H^{7'}$ and $H^{11'}$ ($J_{PH}$ < 1.0 Hz). The $^{15}N$ resonances of the major isomer are observed at $\delta$ = 219.0 ($N^p$), 230.3 ($N^{'p}$), and 236.6 ppm ($N^i$ + $N^a$). By nuclear Overhauser spectroscopy it was possible to elucidate the orientation of one chelate ligand relative to the phosphane. A strong Me ↔ $H^{11}$ contact (between phosphane and ligand L) places the nitrogen atom $N^p$ cis to the phosphane with the $C^{11}{-}H^{11}$ vector pointing in the Mo−P direction, i.e., $N^i$ is located trans to the phosphane. Two further NOE contacts Me ↔ $H^{11'}$ (medium) and Me ↔ $H^{2',6'}$ (medium) are compatible with the OC-6-4-3 and the OC-6-4-4 isomers. From the DFT calculations and NOE contacts we propose again the OC-6-4-3 isomer as the major isomer (compatible with all NOE contacts but not unambiguous). The other (minor) stereoisomer observed is most likely the OC-6-3-3 isomer from an energetic point of view.[8] In the infrared spectrum of complex $\mathbf{4}^{t\mathbf{Bu}}$ absorption of the Mo═O stretching vibration is observed at 935 $cm^{-1}$. For the model $\mathbf{4}^{\mathbf{H}}$ complexes the energies are calculated (and scaled by 0.9614[37]) as 935, 937, 956, and 957 $cm^{-1}$ for isomers OC-6-4-3, OC-6-3-3, OC-6-3-4, and OC-6-4-4, respectively. These data also fit to OC-6-4-3 and OC-6-3-3 stereoisomers. One stereoisomer of $\mathbf{4}^{t\mathbf{Bu}}$ crystallized from THF in the monoclinic space group *C*2/*c* (Tables 1 and 2). As already suggested from combined NMR/DFT analysis the OC-6-4-3 major stereoisomer is indeed present in the crystal (Figure 6, top).

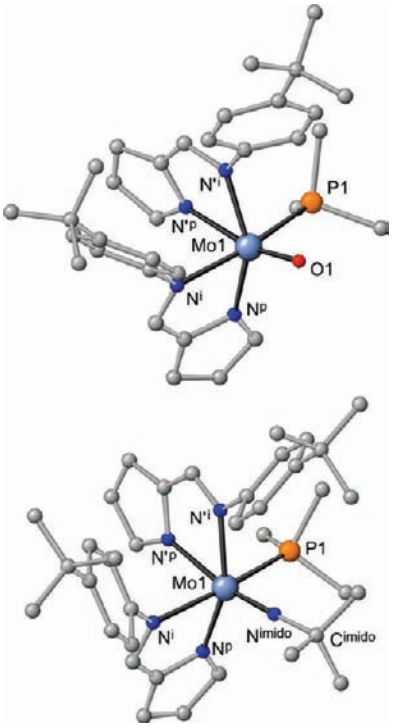


**Figure 6.** Molecular structures of $\mathbf{4}^{t\mathbf{Bu}}$ and $\mathbf{5}^{t\mathbf{Bu}}$ in the crystal (CH hydrogen atoms omitted for clarity).

Reaction of imido complex $\mathbf{2}^{t\mathbf{Bu}}$ with $PMe_3$ (Scheme 1) yields a single molybdenum(IV) phosphane complex $\mathbf{5}^{t\mathbf{Bu}}$ with $\delta(^{31}P)$ = 9.2 ppm and $\delta(^{15}N)$ = 212.0 ($N^p$), 231.1 ($N^{'p}$), 234.2 ($N^i$), and 252.2 ppm ($N^a$) NMR spectral characteristics. The imido nitrogen nucleus experiences the largest shift from $\delta$ = 477.4 ppm ($\mathbf{2}^{t\mathbf{Bu}}$) to $\delta$ = 273.7 ppm ($\mathbf{5}^{t\mathbf{Bu}}$). The $H^7$ resonance of $\mathbf{5}^{t\mathbf{Bu}}$ is split into a doublet by coupling to $^{31}P$ ($^4J_{PH}$ = 2.8 Hz). In the P−H correlation spectrum a weak correlation peak ($J_{PH}$ < 1.0 Hz) is also found to $H^{11'}$ similar to the oxido phosphane complex $\mathbf{4}^{t\mathbf{Bu}}$ (see Supporting Information, Figure S9).

The larger imido ligand in $\mathbf{2}^{t\mathbf{Bu}}$ should disfavor nucleophilic attack of the phosphane at the oxido ligand as compared to reaction of $PMe_3$ with $\mathbf{1}^{t\mathbf{Bu}}$. DFT calculations on $\mathbf{1}^{\mathbf{H}}$ and $PMe_3$ give a barrier of 64.6 kJ $mol^{-1}$,[8] while with $\mathbf{2}^{\mathbf{H}}$ the calculated barrier indeed increases to 108.3 kJ $mol^{-1}$. In addition, the barrier calculated for dissociation of the coordinated phosphane


dx.doi.org/10.1021/ic202588u | *Inorg. Chem.* 2012, 51, 4180−4192

oxide amounts to only 26.3 kJ mol$^{-1}$ in the case $\mathbf{1}^{H}$/PMe$_3$[8] and is almost doubled in the case $\mathbf{2}^{H}$/PMe$_3$ (50.1 kJ mol$^{-1}$). In spite of these decelerating effects the overall phosphane complex formation $\mathbf{2}^{tBu}$ + 2 PMe$_3$ → $\mathbf{5}^{tBu}$ + OPMe$_3$ proceeds roughly 10 times *faster* than the reaction $\mathbf{1}^{tBu}$ + 2 PMe$_3$ → $\mathbf{4}^{tBu}$ + OPMe$_3$ at room temperature as judged by $^{31}$P{$^1$H} NMR spectroscopic reaction monitoring (see Supporting Information, Figure S2). This apparent discrepancy can be ascribed to the absence of dimer accumulation in the imido case as the steric bulk of the imido ligand prevents intermediate formation of imido- or oxido-bridged dimers with six-coordinate molybdenum centers.[38] In the oxido case dimerization retards formation of the phosphane complex $\mathbf{4}^{tBu}$. Thus, in the *overall* reaction the less sterically hindered complex $\mathbf{1}^{tBu}$ reacts slower due to the comproportionation equilibrium to $\mathbf{3}^{tBu}$.

Mösch-Zanetti et al. also observed formation of an imido phosphane complex by reaction of their bis(*β*-ketiminato)(imido)(oxido) complexes **B** (Chart 1) with PMe$_3$ ($\delta$($^{31}$P) = 6.5 ppm). They suggested formation of a stereoisomer in which the oxido ligand is replaced by the phosphane without isomerization in the five-coordinate intermediate. However, no experimental evidence for this stereochemical assignment has been given.[11] In our system DFT calculations on possible stereoisomers of $\mathbf{5}^{H}$ find the OC-6-4-3 isomer as the global minimum and the OC-6-4-4 and OC-6-3-3 isomers 9.8 and 13.6 kJ mol$^{-1}$ higher in energy, respectively (Figure 7). Nuclear

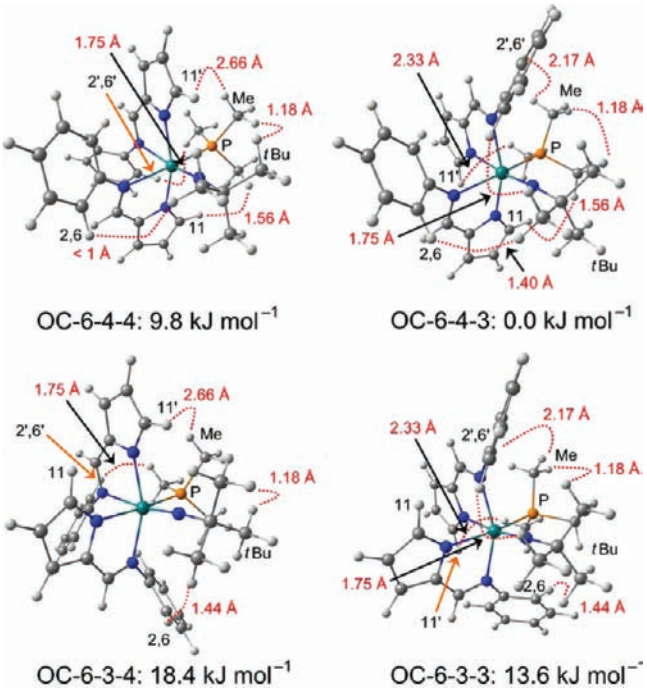


**Figure 7.** DFT-calculated stereoisomers of $\mathbf{5}^{H}$ together with relevant interligand H···H distances (shortest distance obtained by PMe$_3$, phenyl, and *tert*-butyl rotation) and relative energies in kJ mol$^{-1}$.

Overhauser spectroscopy experimentally clarifies the stereochemistry of $\mathbf{5}^{tBu}$ as six relevant interligand NOE contacts are observed, namely, three between PMe$_3$ and the chelate ligands (Me ↔ H$^{11}$, Me ↔ H$^{11'}$, Me ↔ H$^{2',6'}$; similar to $\mathbf{4}^{tBu}$), two between N*t*Bu and the chelate ligands (*t*Bu ↔ H$^{2,6}$; *t*Bu ↔ H$^{2',6'}$), and one between PMe$_3$ and N*t*Bu. The Me ↔ N*t*Bu contact places the phosphane cis to the imido ligand. The Me ↔ H$^{11}$ contact locates the nitrogen atoms N$^{p}$ cis and N$^{i}$ trans to the phosphane as found for $\mathbf{4}^{tBu}$. Finally, the imido ligand displays contacts to ortho protons H$^{2,6}$ and H$^{2',6'}$ of both chelate ligands, which places both imino nitrogen atoms N$^{i}$ and N$^{i'}$ in cis positions to the N*t*Bu ligand. These neighborhood relations are only realized in the (energetically most stable) OC-6-4-3 isomer (Figure 7).

Six-coordinate $\mathbf{5}^{tBu}$ crystallized from diethyl ether/acetonitrile in the monoclinic space group $P2_1/n$ (Table 1). As suggested from the unequivocal NMR/DFT analysis the OC-6-4-3 stereoisomer is present in the crystal (Figure 6, bottom). The Mo═N bond length of $\mathbf{5}^{tBu}$ is slightly larger (1.743(2) Å, Table 2) than that of $\mathbf{2}^{tBu}$ (1.731(2) Å, Table 2), which is also reproduced by the DFT calculation ($\mathbf{5}^{H}$, 1.751 Å; $\mathbf{2}^{H}$, 1.746 Å).The imido ligand in $\mathbf{5}^{tBu}$ is almost perfectly linear with Mo═N−C 178.7(2)° (DFT $\mathbf{5}^{H}$ 174.9°). The DFT-calculated Mo═N−C bending deformation potential is much steeper for the Mo$^{IV}$ complex than for the Mo$^{VI}$ complex (see Supporting Information, Figure S1). The P−Mo═N angle in six-coordinate $\mathbf{5}^{tBu}$ is smaller (92.53(6)°) than those found by Gibson et al. in pseudotetrahedral Mo$^{IV}$(N*t*Bu)$_2$(PMe$_3$)(L) complexes (∼100°, L = olefin or acetylene).[39] In the DFT model $\mathbf{5}^{H}$ the angle is calculated as 94.6°, in good agreement with the experimental value. The Mo−P bond length is shorter for the imido derivative $\mathbf{5}^{tBu}$ (2.4532(6) Å) as compared to that of the oxido derivative $\mathbf{4}^{tBu}$ (2.482(2) Å), suggesting a stronger Mo−P dative bond in $\mathbf{5}^{tBu}$. This trend is also reproduced in the DFT calculation ($\mathbf{5}^{H}$, 2.533 Å; $\mathbf{4}^{H}$, 2.642 Å).

Given the fact that two isomers ($\mathbf{4}^{tBu}$) and one isomer ($\mathbf{5}^{tBu}$) are observed instead of a mixture of several isomers points to a thermodynamically driven product distribution. Thus, coordination of PMe$_3$ in $\mathbf{4}^{tBu}$ and $\mathbf{5}^{tBu}$ should be reversible. To probe this $\mathbf{4}^{tBu}$ and $\mathbf{5}^{tBu}$ were treated with 5 equiv of triethylphosphane PEt$_3$ at 293 ($\mathbf{4}^{tBu}$) and 333 K ($\mathbf{5}^{tBu}$), respectively (Scheme 2). Indeed, in the $^{31}$P{$^1$H} NMR spectra (see

**Scheme 2. Phosphane Exchange via Five-Coordinate Intermediates**

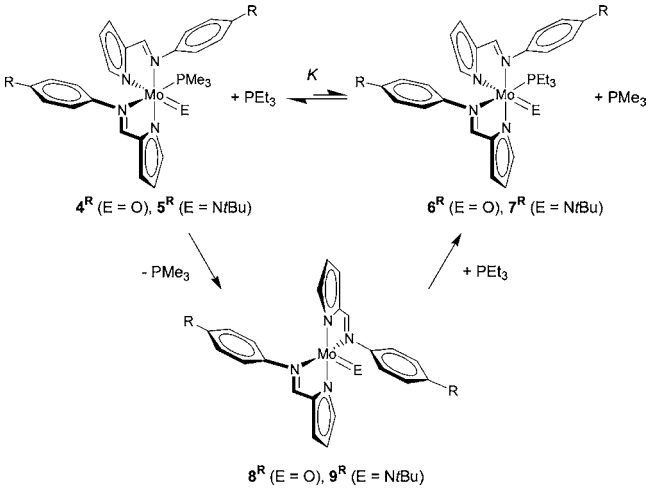


Supporting Information, Figure S10, S11) new resonances at $\delta$ = 23.1 ($\mathbf{4}^{tBu}$/ PEt$_3$) and 33.5 ppm ($\mathbf{5}^{tBu}$/ PEt$_3$) were observed, respectively, together with the resonance of free PMe$_3$ ($\delta$ = −63.1 ppm) and free PEt$_3$ ($\delta$ = −20.1 ppm). The low-field resonances are assigned to the corresponding PEt$_3$ complexes $\mathbf{6}^{tBu}$ and $\mathbf{7}^{tBu}$. The former was also prepared independently by synthesis from $\mathbf{1}^{tBu}$ with PEt$_3$, confirming the assignment. Integration of the resonances assigned to $\mathbf{4}^{tBu}$/$\mathbf{6}^{tBu}$ and $\mathbf{5}^{tBu}$/


dx.doi.org/10.1021/ic202588u | Inorg. Chem. 2012, 51, 4180−4192

$7^{tBu}$ and the free phosphanes allows one to estimate the equilibrium constants as $K_{293} = 12 \times 10^{-3}$ ($4^{tBu}/6^{tBu}$) and $K_{333} = 2 \times 10^{-3}$ ($5^{tBu}/7^{tBu}$). Expectedly, the sterically less encumbered $PMe_3$ complexes are favored due to the smaller Tolman cone angle[40] of $PMe_3$ (118°) as compared to that of $PEt_3$ (132°), which is even more pronounced for the imido complexes $5^{tBu}$ and $7^{tBu}$.

The five-coordinate oxido intermediate $8^H$ has been previously characterized by DFT,[8] and the corresponding calculation of the imido intermediate $9^H$ is presented here (Scheme 2, Supporting Information). The largest calculated N−Mo−N angles of the oxido complex $8^H$ amount to 153.3° and 123.5° describing a geometry between trigonal bipyramidal and tetragonal pyramidal ($\tau = 0.50$[41]), while the corresponding angles in the imido derivative $9^H$ amount to 149.9° and 132.9° describing a more tetragonal pyramidal geometry ($\tau = 0.28$).

Complexes $1^{tBu}$ and $2^{tBu}$ react at different rates in the OAT to $PMe_3$ with the sterically encumbered imido complex $2^{tBu}$ (via $9^{tBu}$) reacting faster than the oxido complex $1^{tBu}$ (via $8^{tBu}$ and then the $\mu$-oxido dimer $3^{tBu}$) as shown by NMR spectroscopy. In a catalytic *double* OAT reaction[42] from dmso to $PMe_3$ giving dimethyl sulfide dms and $OPMe_3$ the imido complex should be the faster catalyst. Initial rates were determined under pseudo-first-order conditions ([$1^{tBu}$], [$2^{tBu}$] = 0.025 mM; $[PMe_3]_0 = 0.25$ mM in dmso) at 298 K (see Supporting Information, Figures S12, S13). Indeed, rate constants of $k_{298} = 1.5(1) \times 10^{-5}$ $s^{-1}$ ($1^{tBu}$) and $k_{298} = 3.0(1) \times 10^{-5}$ $s^{-1}$ ($2^{tBu}$) were determined, confirming the initial faster overall double OAT reactions with the imido system. However, product formation is quantitative only with the oxido but not with the imido catalyst. These findings point to catalyst inhibition during catalysis in the case of $2^{tBu}$. Proton and $^{31}P$ NMR spectroscopy reveal that during turnover of $2^{tBu}$ the phosphane complex $5^{tBu}$ is formed in appreciable amounts, which significantly slows down catalysis (substrate inhibition). No evidence was obtained for formation of a dms complex (product inhibition), which has been recently proposed for the natural enzyme DMSO reductase in the course of turnover.[43] Attempts to displace $PMe_3$ in $5^{tBu}$ by a large excess dimethyl sulfide failed. Furthermore, the phosphane complex $5^{tBu}$ is shown to be stable in the presence of dmso ($^1H$ NMR, $^{31}P\{^1H\}$ NMR) and thus is not a competent catalyst for oxygenation of $PMe_3$ by dmso. Thus, the major reactivity difference between intermediates $8^{tBu}$ and $9^{tBu}$ is their affinity to the molybdenum(VI) catalyst itself ($1^{tBu}/2^{tBu}$) and to the substrate $PMe_3$. The five-coordinate oxido complex $8^{tBu}$ strongly binds to $1^{tBu}$, giving the $\mu$-oxido dimer $3^{tBu}$, while the five-coordinate imido species $9^{tBu}$ preferentially coordinates the substrate $PMe_3$.

The electronic structures of the green $d^2$ complexes $4^{tBu}$ and $5^{tBu}$ were investigated by optical spectroscopy. Both complexes feature several ligand field bands in the visible spectral region, namely, at $\lambda$ = 715 (sh), 610 (sh), and 479 (1420) nm ($4^{tBu}$) and at $\lambda$ = 735 (265), 594 (1000), and 490 (1490) nm ($5^{tBu}$) in THF (Figure 8). TD-DFT calculations find low-energy absorption bands at 728, 659, 453, and 435 nm ($4^H$) and 695, 598, 482, and 458 nm ($5^H$), in reasonable agreement with experiment (Figure 8). The bands are largely composed of $d_{xy} \rightarrow d_{xz}/d_{yz}$ ligand field transitions with some admixture of the chelate and the imido/oxido ligands (Figure 8).

**One-Electron Oxidation of Molybdenum(IV) Complexes to Molybdenum(V) Complexes.** Outer-sphere one-electron oxidation of oxido phosphane complexes $4^R$ (R = $OSiMe_3$) with ferrocenium salts has been previously reported

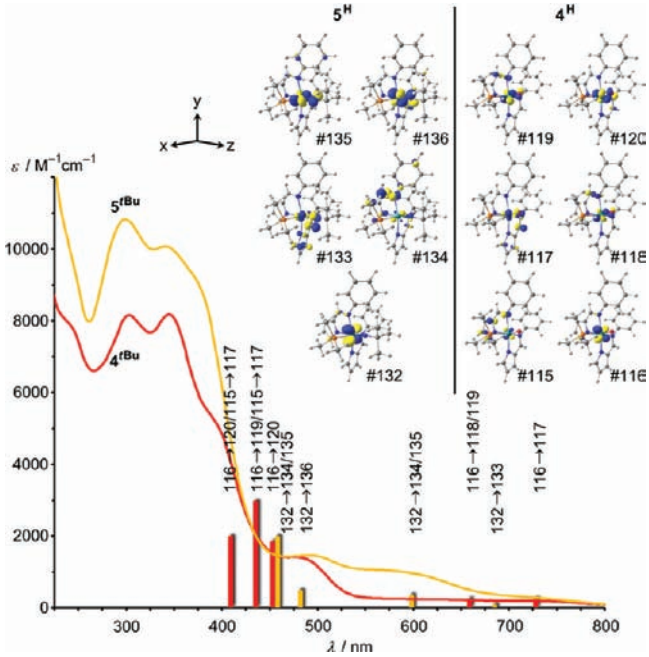


**Figure 8.** UV−vis spectra of $4^{tBu}$ and $5^{tBu}$ in THF; calculated low-energy transitions of $4^H$ and $5^H$ as a stick representation; frontier molecular orbitals of $4^H$ (contour value 0.1 au) and $5^H$ (contour value 0.07 au).

by us.[7,9] It was observed that the larger the coordinated phosphane ligand $PMe_nPh_{3-n}$ ($n$ = 1−3) the more facile the phosphane dissociates from the $Mo^V$ complex.[9] Similarly, the oxido phosphane complex $4^{tBu}$ features only an irreversible oxidation wave in the cyclic voltammogram with $E_p = -0.29$ V vs $FcH/FcH^+$ with a rereduction peak ($E_p = -0.85$ V) clearly associated with a different chemical species (Figure 9, top, left). Higher scan rates or the presence of $PMe_3$ (100 equiv) do not alter the appearance of this cyclic voltammogram significantly. Chemical oxidation of $4^{tBu}$ with ferrocenium hexafluorophosphate gives EPR-active $d^1$ $Mo^V$ species with an average $g_{iso}$ = 1.9459 and $A_{iso}(^{95/97}\text{Mo}) = 49.8$ G ($I(^{95/97}\text{Mo}) = 5/2$). No superhyperfine coupling of the unpaired electron to phosphorus ($I(^{31}P) = 1/2$) is observed, which points to facile dissociation of $PMe_3$ after electron transfer to $Mo^{IV}$ also in this case (Figure 9, top, right). The EPR spectrum in frozen solution at 77 K shows a signal with $g_{1,2,3}$ = 1.9618, 1.9555, and 1.9362 lacking obvious hyperfine splitting (for simulation see Supporting Information, Figure S14) comparable to that of the previously reported Mo(V) complex with $L^{OSiMe3}$ chelate ligands ($g_{1,2,3}$ = 1.9703, 1.9503, 1.9413).[9] Unrestricted DFT geometry optimization on five-coordinate $[4^H]^+$ suggests a geometry between trigonal-bipyramidal and tetragonal pyramidal (largest angles 155.1°, 127.7°; $\tau = 0.46$[41]). Calculated principal $g$ values $g_{1,2,3}$ = 1.9740, 1.9638, and 1.9593 are in reasonably good agreement with the experiment (UB3LYP, WTBS basis set for Mo/EPR-II basis set for C, H, N). However, the presence of other species, e.g., like a THF adduct, or different stereoisomers cannot be excluded on the basis of the EPR spectrum. Such species could also be responsible for the additional peaks in the spectrum, which hampers a reliable simulation of the spectrum (Figure 9, top).

On the other hand, the imido phosphane complex $5^{tBu}$ is *reversibly* oxidized in the cyclic voltammogram at $E_{1/2} = -0.71$ V vs $FcH/FcH^+$ (Figure 9, bottom, left). Simple outer-sphere


dx.doi.org/10.1021/ic202588u | Inorg. Chem. 2012, 51, 4180−4192

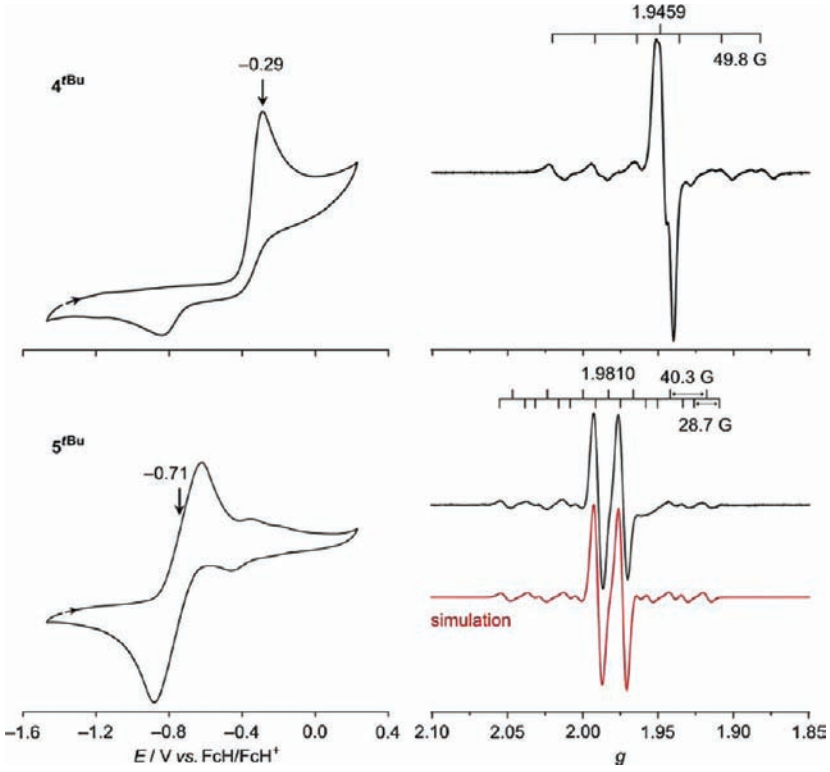


**Figure 9.** Cyclic voltammograms of $\mathbf{4}^{t\mathrm{Bu}}$ and $\mathbf{5}^{t\mathrm{Bu}}$ (left) and X-band CW-EPR spectra of $\mathbf{4}^{t\mathrm{Bu}}$ and $\mathbf{5}^{t\mathrm{Bu}}$ oxidized with $[\mathrm{FcH}](\mathrm{PF}_6)$ at 298 K.

one-electron oxidation of $\mathbf{5}^{t\mathrm{Bu}}$ should retain the stoichiometry and also the OC-6-4-3 stereochemistry. Thus, under these conditions the kinetic six-coordinate $\mathrm{Mo}^{\mathrm{V}}$ product $[\mathbf{5}^{t\mathrm{Bu}}]^+$ with OC-6-4-3 configuration should be formed. This metastable complex should be unable to isomerize to another stereoisomer as trigonal twists are usually quite energy demanding in six-coordinate complexes as long as dissociation is prevented.[44] According to unrestricted DFT calculations the *thermodynamically* most stable stereoisomer $[\mathbf{5}^{\mathrm{H}}]^+$ is the OC-6-4-4 isomer, followed by the OC-6-4-3 isomer (6.3 kJ $\mathrm{mol}^{-1}$), the OC-6-3-4 isomer (11.1 kJ $\mathrm{mol}^{-1}$), and the OC-6-3-3 isomer (16.2 kJ $\mathrm{mol}^{-1}$). To confirm the assumption of formation of the kinetic OC-6-4-3 product $\mathbf{5}^{t\mathrm{Bu}}$ is chemically oxidized with ferrocenium hexafluorophosphate to the $\mathrm{Mo}^{\mathrm{V}}$ complex $[\mathbf{5}^{t\mathrm{Bu}}](\mathbf{PF}_6)$. The isotropic CW EPR spectrum of the product reveals a doublet signal at $g_{\mathrm{iso}} = 1.9810$ with $A_{\mathrm{iso}}(^{31}\mathrm{P}) = 28.7$ G and $A_{\mathrm{iso}}(^{95/97}\mathrm{Mo}) = 40.3$ G (Figure 9, bottom, right). This doublet signal remains stable for days in solution at room temperature. In frozen THF solution the coupling of the unpaired electron to the $^{31}\mathrm{P}$ nucleus is also discernible. Simulation[24] of the rhombic spectrum yields $g_{1,2,3} = 1.9825$, 1.9785, and 1.9615 and $A_{1,2,3}(^{31}\mathrm{P}) = 23$, 33, and 29 G (see Supporting Information, Figure S15). To probe the direct nuclear environment around the central $d^1$ molybdenum ion it is necessary to measure the weak hyperfine couplings (HFC) that are not resolved in the CW EPR spectra. To this end, X-band HYSCORE spectra[45,46] of $[\mathbf{5}^{t\mathrm{Bu}}](\mathbf{PF}_6)$ (Figure 10) in frozen THF solution were recorded at 20 K and analyzed. Experimental details can be found in the Supporting Information. Several off-diagonal cross peaks are detected both in the (−,+) and in the (+,+) quadrant. The HYSCORE data could be satisfactorily simulated[46b] assuming anisotropic couplings to several $^{14}\mathrm{N}$ nuclei. Two weak $^{14}\mathrm{N}$ hyperfine and quadrupolar couplings (see Supporting Information) and one distinctly larger HFC can be inferred

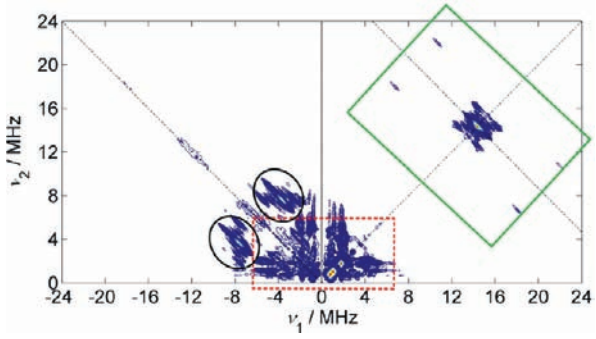


**Figure 10.** X-band HYSCORE spectrum of $[\mathbf{5}^{t\mathrm{Bu}}](\mathbf{PF}_6)$ at 20 K as measured on the maximum of the low-temperature, echo-detected EPR spectrum. $^1\mathrm{H}$ coupling region is marked by a tilted green rectangle, the weak $^{14}\mathrm{N}$ coupling region is marked by a dashed red rectangle, and the main features of the strongly coupled $^{14}\mathrm{N}$ nucleus are marked by black ovals. Detailed spectra and their simulations are shown in Figure S16 in the Supporting Information.

[$A_{1,2,3}(^{14}\mathrm{N}_{\mathrm{small,A}}) = 1.3$, 1.4, 1.7 G, $A_{\mathrm{iso}}(^{14}\mathrm{N}_{\mathrm{small,A}}) = 1.5$ G; $A_{1,2,3}(^{14}\mathrm{N}_{\mathrm{small,B}}) = 0.8$, 0.8, 0.9 G, $A_{\mathrm{iso}}(^{14}\mathrm{N}_{\mathrm{small,B}}) = 0.8$ G; $A_{1,2,3}(^{14}\mathrm{N}_{\mathrm{large}}) = 1.5$, 2.0, 3.8 G, $A_{\mathrm{iso}}(^{14}\mathrm{N}_{\mathrm{large}}) = 2.4$ G]. Furthermore, indirect indications for one strongly coupled proton that may be coupled via a nitrogen atom could be found with $A_{1,2,3}(^1\mathrm{H}) = 3.4$, 4.1, and 5.0 G and $A_{\mathrm{iso}}(^1\mathrm{H}) = 4.2$ G (see Supporting Information[46c]). Note that the $^1\mathrm{H}$ couplings are not directly observed in Figure 10 but by the double-quantum transitions of $^1\mathrm{H}$ and a $^{14}\mathrm{N}$ nucleus. This can be explained by cross-suppression of the $^1\mathrm{H}$ coupling through nuclei with large modulation amplitudes such as $^{14}\mathrm{N}$ and is explained in detail in ref 46c. All hyperfine and quadrupole couplings derived from the simulations are summarized in Table S1 in the Supporting Information.


dx.doi.org/10.1021/ic202588u | *Inorg. Chem.* 2012, 51, 4180−4192

Table 3. Characteristic EPR Data Calculated for the Stereoisomers of $[5^{H}]^{+}$ and Experimental Data for $[5^{tBu}](PF_6)$

| | $g_{iso}$ | $g_{1,2,3}$ | $A_{iso}(^{31}P)$/G | $A_{iso}(^{14}N^{imido})$/G | $A_{iso}(^{1}H)$/G (largest) |
|---|---|---|---|---|---|
| OC-6-4-4 | 1.9755 | 1.9813, 1.9766, 1.9686 | 22.9 | 3.3 | 1.2/1.7 ($H^{9'}$, $H^{10'}$) |
| OC-6-4-3 | 1.9728 | 1.9822, 1.9759, 1.9603 | 25.2 | 4.0 | 2.1 ($H^{11'}$) |
| OC-6-3-4 | 1.9748 | 1.9813, 1.9733, 1.9700 | 27.7 | 3.4 | 1.2/1.5 ($H^{9'}$, $H^{10'}$) |
| OC-6-3-3 | 1.9822 | 1.9845, 1.9824, 1.9798 | 28.4 | 3.1 | 2.2 ($H^{11'}$) |
| exp | 1.9810 | 1.9825, 1.9785, 1.9615 | 28.7[a] | 2.4[b] | 4.2[c] |

[a] $A_{iso}$ is extracted from the X-band CW EPR spectrum. [b] $A_{iso}$ is calculated as the average value of the full hyperfine coupling matrix extracted from the HYSCORE spectrum, not taking into account quadrupolar couplings. [c] This value is inferred from the double-quantum transitions of one $^{14}N$ and one $^{1}H$ from the HYSCORE spectrum.[46c]

EPR parameters $g_{iso}$, $g_{1,2,3}$, $A_{iso}(^{31}P, ^{14}N, ^{1}H)$ have been calculated by DFT (UB3LYP, WTBS basis set for Mo, 6-311++G(2d,2p) basis set for P and EPR-II basis set for C, H, N) for the four different isomers of $[5^{H}]^{+}$ (Table 3). Calculated $g_{iso}$ values of the stereoisomers are very similar, impeding any reliable assignment, while the anisotropic data fit best to the OC-6-4-3 isomer. In all stereoisomers the imido nitrogen nucleus $N^{imido}$ is strongly coupled to the unpaired electron with $A_{iso}(^{14}N^{imido})$ = 3.1−4.0 G, while the other nitrogen atoms of the chelate ligands give rise to smaller couplings with $A_{iso}(^{14}N^{i,p})$ = 0.2−2.1 G. This compares nicely with the experimental HFC data but does not allow distinguishing between the isomers with certainty. Significant couplings to protons with $A_{iso}(^{1}H)$ > 1.0 G are calculated for protons of one pyrrolato ring ($H^{9'}$, $H^{10'}$, $H^{11'}$) with the largest ones found for the OC-6-4-3 and OC-6-3-3 isomers ($A_{iso}(^{1}H, H^{11'})$ > 2.0 G). This assignment is in accord with the suggested stereoisomer OC-6-4-3.

Fortunately, crystals of $[5^{tBu}](PF_6)$ grown from THF/petroleum ether 40−60° solution were suitable for X-ray crystallographic analyses (Table 1). The salt $[5^{tBu}](PF_6)$ crystallized in the orthorhombic space group *Pbca* with additional THF solvent molecules in the unit cell. As expected, the OC-6-4-3 stereoisomer is observed in the crystal (Figure 11).

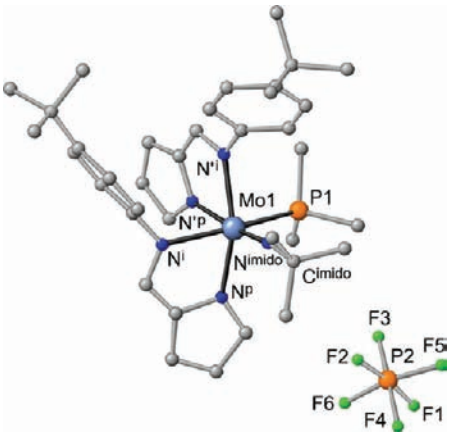


**Figure 11.** Molecular structure of $[5^{tBu}](PF_6)$ in the crystal (CH hydrogen atoms omitted for clarity).

Upon oxidation of $5^{tBu}$ to $[5^{tBu}](PF_6)$ the Mo1−P1 bond length is elongated from 2.4532(6) to 2.549(1) Å (Table 2), while the Mo1=$N^{imido}$ distance remains almost constant ($5^{tBu}$, 1.743(2) Å; $[5^{tBu}](PF_6)$, 1.739(3) Å). In the cation the Mo1=$N^{imido}$−$C^{imido}$ angle is slightly more bent (172.8(3)°) than in the neutral complex (178.8(2)°). The calculated Mo=N−C bending deformation potential for the $d^1$ $Mo^{V}$ complex is very similar to that of the $d^2$ $Mo^{IV}$ complex, suggesting steric rather than electronic reasons for the ligand coordination mode in this system (see Supporting Information, Figure S1).

The magnetic susceptibility $\chi$ of $[5^{tBu}](PF_6)$ was measured in $d_8$-THF at room temperature by the Evans method.[47,48] The experimental magnetic moment $\mu_{eff}$ = 2.828 $(\chi T)^{1/2}$ = 1.71 ± 0.05 $\mu$B corresponds to one unpaired electron ($S$ = 1/2; $\mu_{eff,expected} = g \times (S(S+1))^{1/2}$ = 1.716 $\mu$B[49]).

In the UV−vis spectrum of $[5^{tBu}](PF_6)$ in THF several low-energy absorptions can be distinguished, namely, at 787 ($\varepsilon$ = 905 $M^{-1}$ $cm^{-1}$) and 532 (sh, 1165 $M^{-1}$ $cm^{-1}$) nm, which account for the dark color (Figure 12). TD-DFT calculation on

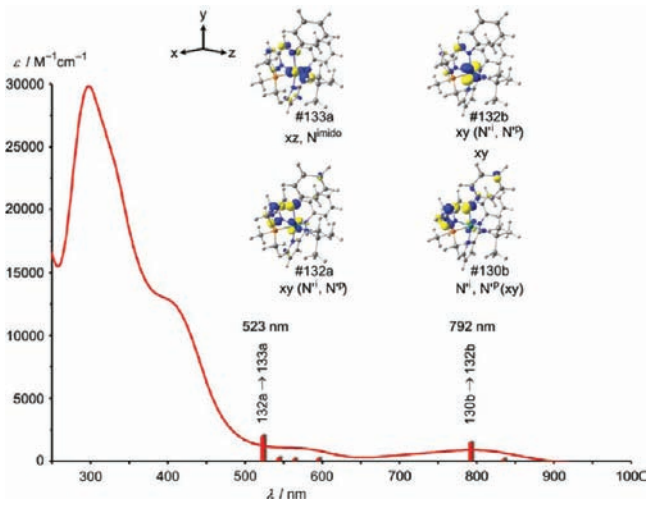


**Figure 12.** UV−vis spectrum of $[5^{tBu}](PF_6)$ in THF; calculated low-energy transitions of $5^{H}$ as a stick representation; relevant frontier molecular orbitals of $5^{H}$ (contour value 0.07 au).

$[5^{H}]^{+}$ assigns the stronger low-energy absorption ($\lambda_{calcd}$ = 792 nm) mainly to a ligand-to-metal charge transfer from the L′ chelate ligand (MO no. 130b) to the singly occupied $d_{xy}$ orbital (MO no. 132b). The second low-energy absorption band is assigned to a ligand field transition from the singly occupied $d_{xy}$ orbital (MO no. 132a) to the $d_{xz}$ orbital ($\pi^*$ orbital, MO no. 133a) with some contribution of $N^{imido}$ ($\lambda_{calcd}$ = 523 nm).

## CONCLUSIONS

Molybdenum(VI) dioxido ($1^{tBu}$) and mixed imido/oxido complexes ($2^{tBu}$) were prepared and fully characterized with respect to stereochemistry (OC-6-4-4), optical properties, and reactivity toward phosphanes as oxygen atom acceptors. Counterintuitively, the sterically more demanding imido ligand promotes a faster overall reaction. The final molybdenum(IV) products $4^{tBu}$ and $5^{tBu}$ of the OAT reactions were isolated, and


dx.doi.org/10.1021/ic202588u | Inorg. Chem. 2012, 51, 4180−4192

their OC-6-4-3 stereochemistry was confirmed by NMR analysis, X-ray diffraction, and DFT calculations. In a catalytic *double* OAT reaction[42] from dmso to $PMe_3$ giving dms and $OPMe_3$ the imido complex $\mathbf{2}^{t\mathrm{Bu}}$ is initially approximately twice as fast as the oxido complex $\mathbf{1}^{t\mathrm{Bu}}$. However, inhibition by the substrate prevents full conversion with the imido catalyst $\mathbf{2}^{t\mathrm{Bu}}$. The optical properties of the $d^2$ complexes $\mathbf{4}^{t\mathrm{Bu}}$ and $\mathbf{5}^{t\mathrm{Bu}}$ were analyzed by TD-DFT calculations, and the low-energy absorptions were assigned $d_{xy} \rightarrow d_{xz}/d_{yz}$ transitions with some admixture of the chelate and the imido/oxido ligands. One-electron oxidation gives the corresponding $d^1$ molybdenum(V) complexes. The oxido phosphane complex is unstable with respect to dissociation of coordinated phosphane ($[\mathbf{4}^{t\mathrm{Bu}}]^+$), while the imido phosphane complex $[\mathbf{5}^{t\mathrm{Bu}}]^+$ has been isolated and fully characterized. The higher stability of the Mo−P bond in $\mathbf{5}^{t\mathrm{Bu}}$ and $[\mathbf{5}^{t\mathrm{Bu}}]^+$ as compared to $\mathbf{4}^{t\mathrm{Bu}}$ and $[\mathbf{4}^{t\mathrm{Bu}}]^+$ is most likely due to electronic rather than steric reasons. The OC-6-4-3 stereochemistry is retained in the molybdenum(V) complex. The unpaired electron in $[\mathbf{5}^{t\mathrm{Bu}}]^+$ couples to the metal center ($^{95/97}$Mo), to the coordinated $^{31}$P nucleus (CW EPR), as well as to $^{14}$N and $^{1}$H of the ligands (HYSCORE). The optical absorption bands of $[\mathbf{5}^{t\mathrm{Bu}}]^+$ are assigned to ligand field and charge transfer transitions. In conclusion, the imido/oxido $\pi$-donor ligands dramatically control the reactivity and stability of the reported Schiff base molybdenum complexes. The reactivity of the novel six-coordinate imido phosphane $Mo^{IV}$ and $Mo^{V}$ complexes is currently investigated in greater detail, especially with respect to exploiting the latent free coordination site by removing the phosphane.

## ■ ASSOCIATED CONTENT

### Ⓢ Supporting Information

Energy profile of the Mo═N−C bending deformation in $\mathbf{2}^{\mathrm{H}}$, $\mathbf{5}^{\mathrm{H}}$, and $[\mathbf{5}^{\mathrm{H}}]^+$ obtained by DFT calculation fixed Mo═N−C angle and optimized geometry; $^{31}P\{^1H\}$ NMR reaction monitoring of the reactions $\mathbf{1}^{t\mathrm{Bu}}$ + $PMe_3$ and $\mathbf{2}^{t\mathrm{Bu}}$ + $PMe_3$ in THF at room temperature; NH-HMBC of $\mathbf{1}^{t\mathrm{Bu}}$, $\mathbf{2}^{t\mathrm{Bu}}$, $\mathbf{4}^{t\mathrm{Bu}}$, and $\mathbf{5}^{t\mathrm{Bu}}$ in $d_8$-THF; PH-COSY of $\mathbf{4}^{t\mathrm{Bu}}$ and $\mathbf{5}^{t\mathrm{Bu}}$ in $d_8$-THF; $^{31}P\{^1H\}$ NMR of the equilibrium reaction $\mathbf{4}^{t\mathrm{Bu}}$ + $5PEt_3$ in $d_8$-THF at 298 K; $^{31}P\{^1H\}$ NMR of the equilibrium reaction $\mathbf{5}^{t\mathrm{Bu}}$ + $5PEt_3$ in $d_8$-THF at 333 K; plots of $[PMe_3]$ vs time and $[PMe_3]/[PMe_3]_0$ vs time for the reaction between $d_6$-dmso and $PMe_3$ catalyzed by $\mathbf{1}^{t\mathrm{Bu}}$ at 298 K; plots of $[PMe_3]$ vs time and $[PMe_3]/[PMe_3]_0$ vs time for the reaction between $d_6$-dmso and $PMe_3$ catalyzed by $\mathbf{2}^{t\mathrm{Bu}}$ at 298 K; X-band EPR spectra of $[\mathbf{4}^{t\mathrm{Bu}}](\mathbf{PF_6})$ and $[\mathbf{5}^{t\mathrm{Bu}}](\mathbf{PF_6})$ in frozen THF at 77 K and simulation; Cartesian coordinates of DFT-optimized complexes. This material is available free of charge via the Internet at http://pubs.acs.org.

## ■ AUTHOR INFORMATION


### Corresponding Author

*Fax: +49-6131-39-27277. E-mail: katja.heinze@uni-mainz.de.


### Notes

The authors declare no competing financial interest.

## ■ ACKNOWLEDGMENTS

We thank the Deutsche Forschungsgemeinschaft for continuously supporting our work. We are grateful to Dr. Mihail Mondeshki for excellent NMR support, Regine Jung-Pothmann for X-ray data collection, and Dr. Andreas Fischer for exploratory experimental work.

## ■ REFERENCES


(1) Holm, R. *Chem. Rev.* **1987**, *87*, 1401−1449.
(2) Hille, R. *Chem. Rev.* **1996**, *96*, 2757−2816.
(3) Hille, R. *Trends Biochem. Sci.* **2002**, *27*, 360−367.
(4) John H. Enemark, J. H.; Cooney, J. J. A.; Wang, J.-J.; Holm, R. H. *Chem. Rev.* **2004**, *104*, 1175−1200.
(5) Schulzke, C. *Eur. J. Inorg. Chem.* **2011**, 1189−1199.
(6) Feng, C.; Tollin, G.; Enemark, J. H. *Biochim. Biophys. Acta* **2007**, *1774*, 527−539.
(7) Heinze, K.; Fischer, A. *Eur. J. Inorg. Chem.* **2007**, 1020−1026.
(8) Heinze, K.; Marano, G.; Fischer, A. *J. Inorg. Biochem.* **2008**, *102*, 1199−1211.
(9) Heinze, K.; Fischer, A. *Eur. J. Inorg. Chem.* **2010**, 1939−1947.
(10) Lyashenko, G.; Saischek, G.; Judmaier, M. E.; Volpe, M.; Baumgartner, J.; Belaj, F.; Jancik, V.; Herbst-Irmer, R.; Mösch-Zanetti, N. C. *Dalton Trans.* **2009**, 5655−5665.
(11) Mösch-Zanetti, N. C.; Wurm, D.; Volpe, M.; Lyashenko, G.; Harum, B.; Belaj, F.; Baumgartner, J. *Inorg. Chem.* **2010**, *49*, 8914−8921.
(12) Ramnauth, R.; Al-Juaid, S.; Motevalli, M.; Parkin, B. C.; Sullivan, A. C. *Inorg. Chem.* **2004**, *43*, 4072−4079.
(13) The stereochemistry of the complexes under study will be described by the configuration index according to the Cahn−Ingold−Prelog system in an octahedral complex OC-6-*x*-*y* with the priority sequence used as follows: $PMe_3 > O > N^{imido} > N^{pyrrolato} > N^{imine}$. The first index *x* refers to the ligand priority of the ligand trans to the ligand of the highest priority (axial ligands), and the second index *y* refers to the ligand priority trans to the ligand of the equatorial plane which has the highest priority of these four equatorial ligands. Thus, molybdenum(VI) complexes $\mathbf{1}^{\mathrm{R}}$ and $\mathbf{2}^{\mathrm{R}}$ possess OC-6-4-4 stereochemistry, while molybdenum(IV) complexes $\mathbf{4}^{\mathrm{R}}$ and $\mathbf{5}^{\mathrm{R}}$ are OC-6-4-3 stereoisomers as depicted in Scheme 1. For the sake of better comparison with $\mathbf{2}^{\mathrm{R}}$ we enumerated both oxido ligands in $\mathbf{1}^{\mathrm{R}}$. Correctly, the preferred isomer of $\mathbf{1}^{\mathrm{R}}$ should be described by OC-6-3-3 as there is no distinguished fourth donor atom present.
(14) Cahn, R. S.; Ingold, C. K.; Prelog, V. *Angew. Chem., Int. Ed. Engl.* **1966**, *5*, 385−415.
(15) Prelog, V.; Helmchen, G. *Angew. Chem., Int. Ed. Engl.* **1982**, *21*, 567−583.
(16) Block, B. P.; Powell, W. H.; Fernelius, W. C. *Inorganic chemical nomenclature:principles and practice*; ACS Professional Reference Book; American Chemical Society: Washington, DC, 1990.
(17) von Zelewsky, A. *Stereochemistry of Coordination Compounds*: John Wiley & Sons Ltd.: New York, 1996.
(18) Cross, W. B.; Anderson, J. C.; Wilson, C. S. *Dalton Trans.* **2009**, 1201−1205.
(19) Cross, W. B.; Anderson, J. C.; Wilson, C.; Blake, A. J. *Inorg. Chem.* **2006**, *45*, 4556−4561.
(20) Gibson, V. C.; Graham, A. J.; Jolly, M.; Mitchell, J. P. *Dalton Trans.* **2003**, 4457−4465.
(21) Radius, U.; Wahl, G.; Sundermeyer, J. *Z. Anorg. Allg. Chem.* **2004**, *630*, 848−857.
(22) Rufanov, K. A.; Zarubin, D. N.; Ustynyuk, N. A.; Gourevitch, D. N.; Sundermeyer, J.; Churakov, A. V.; Howard, J. A. K. *Polyhedron* **2001**, *20*, 379−385.
(23) Merkoulov, A.; Harms, K.; Sundermeyer, J. *Eur. J. Inorg. Chem.* **2005**, 4902−4906.
(24) Stoll, S.; Schweiger, A. *J. Magn. Reson.* **2006**, *178*, 42−55.
(25) *SMART Data Collection and SAINT-Plus Data Processing Software for the SMART System (various versions)*; Bruker Analytical X-Ray Instruments, Inc.: Madison, WI, 2000.
(26) Blessing, B. *Acta Crystallogr.* **1995**, *A51*, 33−38.
(27) Sheldrick, G. M. *SHELXTL*, Version 5.1; Bruker AXS: Madison, WI, 1998.
(28) Sheldrick, G. M. *SHELXL-97*; University of Göttingen, Göttingen, Germany, 1997.
(29) Frisch, M. J.; Trucks, G. W.; Schlegel, H. B.; Scuseria, G. E.; Robb, M. A.; Cheeseman, J. R.; Montgomery, J. A.; Vreven, Jr., T.; Kudin, K. N.; Burant, J. C.; Millam, J. M.; Iyengar, S. S.; Tomasi, J.;

Barone, V.; Mennucci, B.; Cossi, M.; Scalmani, G.; Rega, N.; Petersson, G. A.; Nakatsuji, H.; Hada, M.; Ehara, M.; Toyota, K.; Fukuda, R.; Hasegawa, J.; Ishida, M.; Nakajima, T.; Honda, Y.; Kitao, O.; Nakai, H.; Klene, M.; Li, X.; Knox, J. E.; Hratchian, H. P.; Cross, J. B.; Adamo, C.; Jaramillo, J.; Gomperts, R.; Stratmann, R. E.; Yazyev, O.; Austin, A. J.; Cammi, R.; Pomelli, C.; Ochterski, J. W.; Ayala, P. Y.; Morokuma, K.; Voth, G. A.; Salvador, P.; Dannenberg, J. J.; Zakrzewski, V. G.; Dapprich, S.; Daniels, A. D.; Strain, M. C.; Farkas, O.; Malick, D. K.; Rabuck, A. D.; Raghavachari, K.; Foresman, J. B.; Ortiz, J. V.; Cui, Q.; Baboul, A. G.; Clifford, S.; Cioslowski, J.; Stefanov, B. B.; Liu, G.; Liashenko, A.; Piskorz, P.; Komaromi, I.; Martin, R. L.; Fox, D. J.; Keith, T.; Al-Laham, M. A.; Peng, C. Y.; Nanayakkara, A.; Challacombe, M.; Gill, P. M. W.; Johnson, B.; Chen, W.; Wong, M. W.; Gonzalez, C. Pople, J. A. *Gaussian 03*, Revision B.03; Gaussian, Inc.: Pittsburgh, PA, 2003.

(30) Huzinaga, S.; Andzelm, J.; Klobukowski, M.; Radzio-Andzelm, E.; Sakai, Y.; Tatewaki, H. *Gaussian Basis Sets for Molecular Orbital Calculations*; Elsevier: Amsterdam, 1984.

(31) Barone, V. In *Recent Advances in Density Functional Methods*; Chong, D. P., Ed.; World Scientific: Singapore, 1995; Part 1.

(32) The WTBS basis set was obtained from the Extensible Computational Chemistry Environment Basis Set Database, Version 02/02/06, as developed and distributed by the Molecular Science Computing Facility, Environmental and Molecular Sciences Laboratory, which is part of the Pacific Northwest Laboratory, P.O. Box 999, Richland, WA 99352, and funded by the U.S. Department of Energy. The Pacific Northwest Laboratory is a multiprogram laboratory operated by the Battelle Memorial Institute of the U.S. Department of Energy under Contract DE-AC06-76RLO.

(33) $R^x_y(n)$: The superscript $x$ denotes the number of hydrogen acceptors, the subscript $y$ the number of hydrogen donors, and $n$ the ring size.

(34) Bernstein, J.; Davis, R. E.; Shimoni, L.; Chang, N.-L. *Angew. Chem., Int. Ed. Engl.* **1995**, *34*, 1555−1573.

(35) Ciszewski, J. T.; Harrison, J. F.; Odom, A. L. *Inorg. Chem.* **2004**, *43*, 3605−3617.

(36) Korn, K.; Schorm, A.; Sundermeyer, J. *Z. Anorg. Allg. Chem.* **1999**, *625*, 2125−2132.

(37) Koch, W.; Holthausen, M. C. *A Chemist's Guide to Density Functional Theory*; Wiley-VCH: Weinheim, 2001; p 134.

(38) An imido-bridged $Mo^V$ dimer has been reported, although with five-coordinate molybdenum centers, i.e., with less steric congestion: Ortiz, C. G.; Abboud, K. A.; Boncella, J. M. *Organometallics* **1999**, *18*, 4253−4260.

(39) Dyer, P. W.; Gibson, V. C.; Howard, J. A. K.; Whittle, B.; Wilson, C. *Polyhedron* **1995**, *14*, 103−111.

(40) Tolman, C. A. *Chem. Rev.* **1977**, *77*, 313−348.

(41) Addison, A. W.; Rao, T. N.; Reedijk, J.; van Rijn, J.; Verschoor, G. C. *J. Chem. Soc., Dalton Trans.* **1984**, 1349−1356.

(42) Mayilmurugan, R.; Harum, B. N.; Volpe, M.; Sax, A. F.; Palaniandavar, M.; Mösch-Zanetti, N. C. *Chem. − Eur. J.* **2011**, *17*, 704−713.

(43) Mtei, R. P.; Lyashenko, G.; Stein, B.; Rubie, N.; Hille, R.; Kirk, M. L. *J. Am. Chem. Soc.* **2011**, *133*, 9762−9774.

(44) Bickely, D. G.; Serpone, N. *Inorg. Chem.* **1976**, *15*, 2577−2582.

(45) (a) Höfer, P.; Grupp, A.; Nebenführ, H.; Mehring, M. *Chem. Phys. Lett.* **1986**, *132*, 279−282. (b) Calle, C.; Sreekanth, A.; Fedin, M. V.; Forrer, J.; Garcia-Rubio, I.; Gromov, I. A.; Hinderberger, D.; Kasumaj, B.; Léger, P.; Mancosu, B.; Mitrikas, G.; Santangelo, M. G.; Stoll, S.; Schweiger, A.; Tschaggelar, R.; Harmer, J. *Helv. Chim. Acta* **2006**, *89*, 2495−2521. (c) Schweiger, A.; Jeschke, G. *Principles of Pulsed Electron Paramagnetic Resonance*; Oxford University Press, 2001.

(46) (a) Hinderberger, D.; Piskorski, R.; Goenrich, M.; Thauer, R. K.; Schweiger, A.; Harmer, J.; Jaun, B. *Angew. Chem., Int. Ed.* **2006**, *45*, 3602−3607. (b) Madi, Z.; van Dorslaaer, S.; Schweiger, A. *J. Magn. Reson.* **2002**, *154*, 181−191. (c) Kasumaj, B.; Stoll, S. *J. Magn. Reson.* **2008**, *190*, 233−247.

(47) Evans, D. F. *J. Chem. Soc.* **1959**, 2003−2005.

(48) Sur, S. K. *J. Magn. Reson.* **1989**, *82*, 169−173.

(49) Hare, C. R.; Bernal, I.; Gray, H. B. *Inorg. Chem.* **1962**, *1*, 831−835.